THESIS ON MECHANICAL ENGINEERING E110

High Strength Ductile Aluminium Matrix Composite

KASPAR KALLIP

TTÜ PRESS

TALLINN UNIVERSITY OF TECHNOLOGY

School of Engineering

Department of Mechanical and Industrial Engineering

This dissertation was accepted for the defence of the degree of Doctor of Philosophy in Engineering on 31.10.2017

Supervisors: Lauri Kollo PhD, Department of Mechanical and Industrial Engineering, Tallinn University of Technology

Marc Leparoux PhD, EMPA Swiss Federal Laboratories for Material Science and Technology, Thun, Switzerland.

Opponents: Prof. Filipe Samuel Silva, School of Engineering, University of Minho, Guimaraes, Portugal.

Hanry Yang, PhD, Thin film process engineer, Keysight Technologies, USA

Defence of the thesis: 01.12.2017

Declaration:

Hereby I declare that this doctoral thesis, my original investigation and achievement, submitted for the doctoral degree at Tallinn University of Technology has not been submitted for any academic degree.

ISSN 1406-4758
ISBN 978-9949-83-175-3 (publication)
ISBN 978-9949-83-176-0 (PDF)

MEHHANOTEHNIKA E110

Kõrgtugev ja plastne alumiiniumkomposiitmaterjal

KASPAR KALLIP

TTÜ KIRJASTUS

CONTENTS

LIST OF ABBREVIATIONS

BET – Brunauer, Emmett and Teller (the specific surface area of particle)
BPR – Ball-to-Powder ratio
CFE-SEM – Cold Field Emission Scanning Electron Microscope
CG – Coarse Grain (structure)
CHC – Compaction Heating Cycle
CMC – Ceramic Matrix Composite (material)
CNT – Carbon Nanotube
DTA – Differential Thermal Analysis
EBSD – Electron backscatter diffraction
EMPA – Swiss Federal Laboratories for Materials Science and Technology
EPFL - École polytechnique fédérale de Lausanne
FCC – Face Centred Cubic (structure)
FE-SEM – Field Emission Scanning Electron Microscope
FG – Fine Grain Structure
GB – Grain boundary
GBMA – Grain Boundary Misorientation Angle
HAGB – High Angle Grain Boundary
HIP – Hot Isostatic Pressing
HP – Hot pressing
HR-TEM – High Resolution Transmission Electron Microscope
LAGB – Low Angle Grain Boundary
MA – Mechanical Alloying
MM – Mechanical Milling
MMC – Metal Matrix Composite
MWCNT – Multi Wall Carbon Nanotube
ODS – Oxide Dispersion-Strengthened (alloy)
PCA – Process Control Agent
PMC – Plastic Matrix Composite material
PSI - The Paul Scherrer Institute
SA – Stearic Acid
SEM – Scanning Electron Microscope
SPS – Spark Plasma Sintering
STEM – Scanning Transmission Electron Microscope
TEM – Transmission Electron Microscope
TKD – Transmission Kikuchi Diffraction
TUT – Tallinn University of Technology
UTS – Ultimate Tensile Strength
VGCF – Vapour Grown Carbon Fibre
XRD – X-ray Diffraction
YS – Yield Strength

INTRODUCTION

The hunt for high strength, lightweight materials has been major topic during last centuries. Aerospace, automotive, electronics, and renewable energy are only few fields where the advantages of using lighter and stronger materials are crucial. With the possibility to increase the strength and stiffness of materials, the mass of required material for certain load bearing application decreases. This has led to several advantages in automotive and aviation industries enabling larger payloads with better fuel efficiency [1].

The author of present study focuses on improving the strength and ductility of aluminium based metal matrix composites and on achieving that with minimal processing steps. The thesis consists of four main chapters. The first chapter introduces the background and structure of thesis. The state of art of literature is described and objectives of the study are stated.

The second chapter introduces the materials selections and employed fabrication technologies. The characterisation methods and equipment are introduced.

The third chapter consist of five subsections. The first section is dedicated to the study of matrix alloys, where 4 commercially available aluminium alloys are reinforced with the same Carbon Nano Tube (CNT) reinforcement to identify the suitable alloy for high strength Metal Matrix Composite (MMC). The second subsection is dedicated to study of reinforcements, where AlMg5 alloy is strengthened with different CNT and Al_2O_3 based nanoparticulates. The third subsection describes the novel cube milling system and benefits of using rectangular milling vessel. It also describes the possibility of producing high strength near net shaped Al-MMCs by uniaxial hot pressing.

The fourth subsection is dedicated to strengthening mechanisms and their major role in achieving high strength with simultaneous ductility.

The fifth subsection presents the study of compaction methods other than hot pressing to compact nanocomposite powders.

The main results of present thesis have been published in 4 pre-reviewed journals and presented in 3 international conferences.

1. LITERATURE OVERVIEW

The alloying of metals has provided higher strength than before, but the inadequacy of metals and alloys to provide desirable strength and stiffness simultaneously has led to the development of composite materials. Composites are engineering materials that have a combination of two or more different materials that share clear interface between them with the intention of tailoring different desired properties for materials. These materials are referred to as the matrix and reinforcement. The matrix being metal, ceramic or polymer and the reinforcement (usually less than 50% of the whole material) normally being of different nature than the matrix. Depending on the matrix, the composites are known as metal matrix composites (MMCs) if the matrix is made out of metallic material, or polymer matrix composites (PMCs) and ceramic matrix composites (CMCs) depending of the nature of matrix material.

In the present work, only MMCs are considered. In MMCs the toughness and ductility is provided by the ductile metal matrix while the strength and stiffness is provided by the reinforcement that is either ceramic, high strength metal based particulates or different fibres [2, 3]. Particulate reinforced MMCs are especially of great interest due to their isotropic properties. Additionally particulate reinforced MMCs are easier and often cheaper to manufacture than continuous fibre reinforced MMCs.

1.1 Mechanical alloying and milling

Mechanical alloying (MA) is a powder processing technique first used around 1966 in order to create nickel oxide-dispersion strengthened (ODS) superalloys [3]. These ODS superalloys are commonly considered as the first type of nanocomposites developed by mechanical alloying. The process of mechanical alloying is a solid-state powder processing technique involving repetitive cold welding, fracturing and rewelding of powder particles in a high-energy ball mill. In this process a specific quantity of powder mixture is loaded into a container along with grinding media (typically chromium steel or hardmetal balls) and agitated to induce repetitive ball impacts on powder.

In the case of metal matrix composites the components can be produced using mechanical milling (MM), during which the ductile metal and brittle reinforcement are mixed. The process is referred as ductile-brittle system and the milling in this process takes place as follows. The initial ball impact causes the ductile metal particles to flatten and consequently work harden due to plastic deformation. The brittle particles on the other hand will undergo fragmentation during the initial impacts (Fig. 1). After initial impacts the fragmented brittle particles get trapped between flattened ductile particles, and with continuous new impacts, the cold welding will take place. With the ongoing cold welding the

particles will receive further impacts from milling media and work hardening of matrix will lead to fracturing into equiaxed particles. During rewelding and fracturing the dispersion of reinforcement takes place, leading to effective second phase reinforcement and grain size reduction. The process can be considered finished when desired state of second phase distribution and work hardening of matrix is achieved. During the process of fracturing and rewelding of particles, the ductile matrix has tendency to form clumps of powder due to excessive cold welding. These large clumps are disturbing the milling by inhibiting work hardening and redistribution of second phase particles. To control the excessive cold welding, process control agents (PCA) are used. Typical PCA is mostly organic surface-active compound that adheres to powder surface, thus inhibiting excessive cold welding. Therefore the rewelding and fracturing mechanisms can be optimised with the type and content of PCA, making it one of the must-controlled parameters of MA and MM [4, 5].

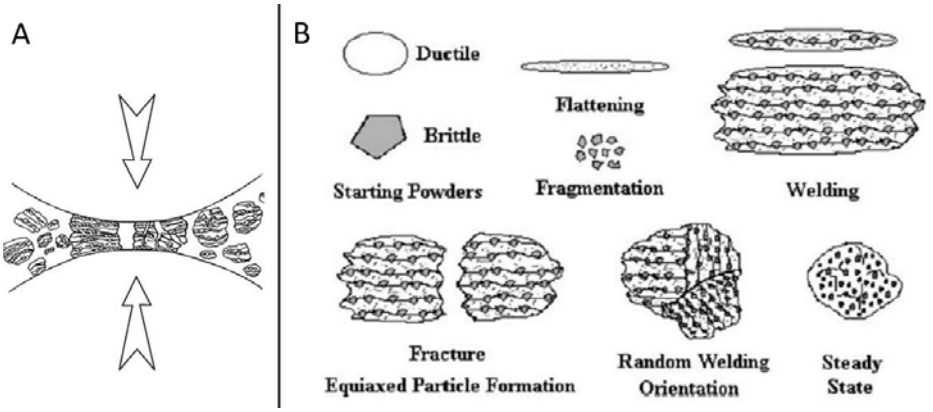

Figure 1. Mechanism of mechanical milling: A) Schematic of a single balls impact on powder [3]; B) Ductile-brittle system of mechanical milling process consisting of flattening and repetitive fragmentation of particles [6]

Optimization of MM process is complex due to number of influencing parameters and variables to achieve desired microstructure and/or desired product properties. Some of the most important parameters to be considered are:

- Type of ball-mill
- Size, shape and material of milling container
- Milling environment (dry, if dry then which atmosphere, wet)
- Milling speed
- Milling time

- Extent of filling the milling container
- Type, size and size distribution of the milling medium (milling balls)
- BPR
- Type and content of PCA
- Temperature of milling

In order to quantify optimum milling efficiency, the concept of milling energy is used. For example Kollo et al. have calculated normalized input energy for Al-SiC MMCs milled with high energy planetary ball-mill. The authors have described the combination of parameters necessary to reach the desired state of milled powders [7].

In MM process different types of mills can be used. In the current work only planetary type ball-mills are considered. Typical planetary ball-mill, accommodating up to few kilograms of powder in one milling cycle gets its name from the planet-like movement of its vessels. The vessels are arranged on rotating support disk and planetary drive mechanism causes them to rotate around their own axes during the movement of support table. The centrifugal forces created by rotating of support disk as well as vessels rotating around their own axes, act on the vessel contents. The rotation of vessels can be either the same as support disk or on opposite direction causing different milling conditions. The grinding balls running the inside wall of vessel, followed by the material being ground and grinding balls lifting off and travelling freely through the vessel colliding against opposing inner wall creating the energy for milling.

1.2 Matrix and reinforcement

Among light metals, aluminium alloys have high specific strength but lack the stiffness necessary in many applications. Extensive investigations have been subjected to further increase the mechanical properties by dispersing particulate materials and especially nanoparticles into the ductile matrices. Most commonly for reinforcement SiC, B_4C, Al_2O_3 and different forms of carbon (carbon nanotubes (CNTs), carbon black and graphene) are selected [2]. Conventionally, micron sized particles have been used to increase the strength of the composite, but recently several authors have proven the supremacy of nano sized reinforcements. The micron sized reinforcement though being effective of increasing materials Young's modulus, have a drawback in terms of fracturing of reinforcement particles during tensile or compressive loading and difficulties in machining [8, 9]. Nano scale reinforcements on other hand have proven to be even more effective for increasing the strength of material without fracturing of particulates. For example Kang et al. reinforced aluminium with micron- and nano-sized Al_2O_3 particles and presented a particular advantage of nanoreinforcement for increasing the strength already at relatively low content [9]. According to them, strengthening effect is increasing with the volume fraction of

reinforcement up to 4 vol. %, above which the strengthening levels off due to the clustering of Al_2O_3 nanoparticles. In comparison, more than 10 vol. % of micron sized reinforcement is normally used to achieve notable increase in mechanical strength [10]. Therefore the application of nano sized reinforcement is in the interest of the author of current work.

Carbon based reinforcements, namely graphite, CNTs and graphene, have also been under investigation by many researchers [2, 11-14]. The outstanding high specific strength of CNTs has made them very popular choice of reinforcement in light metal MMCs. It is possible to disperse several percent of CNTs into aluminium matrix thus increasing significantly the strength [12]. Unfortunately also with CNT reinforcement there are some challenges to overcome before achieving the high-performance composite. Some of the main aspects to consider are achieving a homogeneous distribution of CNTs in matrix material, damaging of the CNTs during high energy milling and the formation of Al_4C_3 during consolidation or heat treatment. There are several reports about prolonged high energy ball milling leading to destruction of CNTs. Liu et al. confirmed this with Raman spectroscopy, showing that the integrated intensity ratio between the G- (graphite) and D-line (defects) of carbon (I_G/I_D) decreases with increasing milling time [13]. Furthermore the authors observed that the improvement of the dispersion uniformity was not obvious after increasing milling time over an optimum, however CNTs damage became more evident. Esawi et al. reported a comparative study of two different CNTs dispersed in an aluminium matrix [14]. They found that cold welding of milled powders as well as aluminium carbide formation in the final composite is depending on the CNTs diameter and morphology. The smaller CNTs having larger interfacial contact area with aluminium matrix were found to reduce particle welding during milling but also to promote the carbide formation. Perez-Bustamante et al. suggested that the formation of Al_4C_3 is the interaction between the outer shells of CNTs and the aluminium matrix during the processing [15]. Lijie et al. have also found that the Al_4C_3 is formed at the interface between the aluminium and CNT layers. More precisely the reaction generally occurred at locations with amorphous carbon such as at defect sites and at open ends of the CNTs. The authors claimed that the carbide formation on the surfaces and on the tips of the CNTs improves the interfacial strength between the CNTs and the aluminium matrix and therefore contributes to the enhancement of the composite mechanical properties [16]. Similar observations were done by Kwon et al. who showed that nano sized Al_4C_3 could offer a beneficial chemical bonding between the aluminium matrix and the CNTs [17]. So with optimized milling parameters the problems mentioned above could be diminished by the tremendous increase of strength while using CNT reinforcement on aluminium based matrix.

1.3 Compaction of blends

After having achieved the desired properties on composite powder blend, the powder must be compacted to harvest its true values. All the consolidation methods generally used in powder metallurgy processes can be used for MM powders. However, due to particles being smaller after MM (typically form a few μm to 100 microns) than those used in conventional powder metallurgy operations, some special precautions need to be taken to minimize their activity (affinity to ignite under air atmosphere) and high level of interparticle friction. Cold compaction is not a favoured option due to mechanically alloyed powders having high hardness (from work hardening). Further, aluminium based ODS alloys do not usually densify during conventional sintering.

Therefore the most common methods of consolidation involves several steps: first to consolidate the powder and second to break the oxide layer covering the metal surfaces of particles by plastic deformation to induce metal-metal contact. Hot compaction followed by hot extrusion, hot isostatic pressing (HIP) followed by hot extrusion and hot compaction followed by hot forging or hot rolling are the most common consolidation methods. The process temperatures are under considerations because the possible loss of metastable effects as well as recrystallization and grain growth of fine grains should be avoided by using process temperatures as low as possible and as high as needed [10].

1.4 Strengthening mechanisms

The increase in strength and hardness of MMCs is usually described by several simultaneous strengthening mechanisms. Commonly the strengthening is accomplished with reducing mobility (gliding) of dislocations. The hindering of dislocation movement is then achieved with the presence of different obstacles such as other dislocations, grain boundaries, solute atoms and precipitates or particles of another phase.

For example, depending on the alloy, the strengthening of alloyed matrix can be described with solid solution strengthening or precipitation strengthening.

Solid solution strengthening is resulting from interaction between the mobile dislocations and the solute atoms in matrix. The presence of solute atoms increases the initial yield stress and reduces the dynamic recovery rate of dislocations. Most commonly, the strengthening of a solid solution is calculated by the correlation between the flow stress and alloy concentration [18]:

$$\sigma_{SS} = \sigma_{pure} + Hc^n, \qquad (1)$$

Where σpure is the flow stress of a pure metal matrix, C is the wt% of solute atoms in alloy and H and n are constants.

In precipitation strengthening, the second phase particles have been introduced to matrix. By means of alloying this is achieved by precipitation from a supersaturated matrix phase via age hardening. The precipitates then act as obstacles that effectively hinder the movement of dislocations. The strengthening effect can then be accounted as Orowan strengthening mechanism.

In the Orowan strengthening mechanism the yield strength of metal is related to the particulate-dislocation interaction. During deformation, dislocation movement through crystal is disturbed by reinforcing second phase particles, leaving residual loops around each reinforcing particle, leading to increased strength [19].The yield strength due to Orowan strengthening (σ_{OR}) can be estimated according to:

$$\sigma_{OR} = M\frac{0.4Gb}{\pi\lambda}\frac{\ln(\frac{2\overline{r}}{b})}{\sqrt{1-u}} \qquad (2)$$

Where *M* is the mean orientation factor (for randomly oriented FCC metals M = 3.06), *G* is the shear modulus of MMC calculated from Young's modulus (Eq. (3)), *b* is the Burger's vector (*b* = 0.286 nm for aluminium), *u* is Poisson's ratio of matrix, $\overline{r}$ is the mean radius of a circular cross section in random plane for a spherical reinforcement particle (Eq. (4)), *r* is the mean radius of reinforcement particle and λ is the interparticle spacing that can be calculated from Eq. (5):

$$G = \frac{E}{2(1+u)} \qquad (3)$$

$$\overline{r} = \sqrt{\frac{2}{3}}r \qquad (4)$$

$$\lambda = 2\overline{r}\left(\sqrt{\frac{\pi}{4f}} - 1\right) \qquad (5)$$

To calculate Orowan strengthening, the particle size distribution of the nanoreinforcement is considered to be monodisperse and its distribution in the matrix homogeneous.

The strengthening due to pile up of dislocations can also lead to strengthening and is calculated using the Taylor formula [20]:

$$\sigma_\rho = M\alpha Gb\sqrt{\rho} \qquad (6)$$

Where M is a mean orientation factor for randomly oriented Face Centred Cubic (FCC) metals, α is a material constant, G is the shear modulus of matrix, b is the Burgers vector and ρ is the dislocation density.

Considering the effect of mechanical milling (MM) on the strength of Al-MMC, then the grain size refinement must be named as one of the main strengthening mechanism. During MM the reduction of grain size increases the number of grain boundaries, which then by blocking the movement of dislocations leads to increased yield strength. The Grain boundary strengthening is described by well-known Hall-Petch relationship [21, 22]:

$$\sigma_{HP} = \sigma_0 + KD^{-1/2} \qquad (7)$$

Where σ_0 is a constant for the starting stress of dislocation movement, K is the Hall-Petch slope and D is the grain diameter.

However, high strength alone is not the sole important parameter for a successful structural material. A structure must be able to support a load and in case of overloading, not to fail catastrophically. Unfortunately, high strength traditionally leads to reduced ductility of material. Therefore, extensive work has been done by many researchers to achieve a material with high strength and acceptable ductility [23–28]. In the case of the strength achieved through the Hall-Petch relationship by creating a fine grained (FG) material (average grain size < 1 μm), the low tensile ductility can be attributed to the premature onset of plastic instability (necking), which in turn is caused by low strain hardening capability. According to the Considère's criterion, strain hardening is needed to delay the tensile necking [29]. Strain hardening classically results from interactions of gliding and intersecting dislocations. Typically, coarse grains (CGs) provide enough spacing for a significant number of dislocation intersections during deformation, while in fine grains there is not enough space for dislocation intersections, ultimately leading to brittle fraction [29]. One possibility would be to combine FGs and CGs into a so-called bi- or trimodal grain structure, which is believed to increase the ductility without sacrificing a substantial amount of strength. Tellkamp et al. proposed a fracture theory where coarse grains in a bimodal grain structure blunt the crack and therefore induce an increased ductility (Fig. 2), [24].

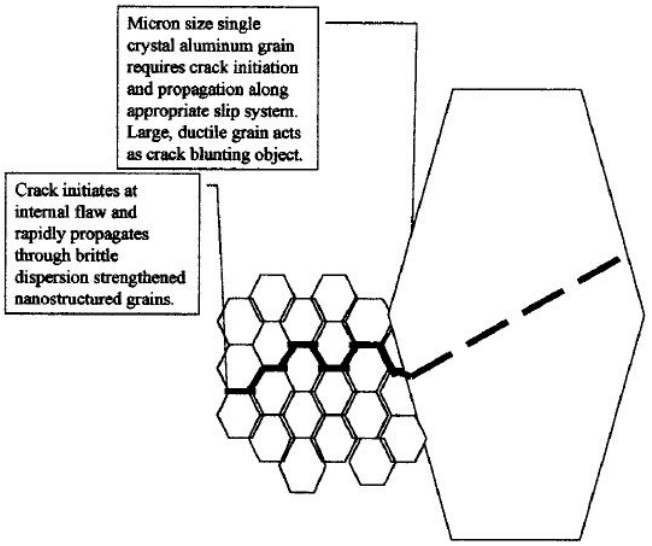

Figure 2. Illustration for theory for enhanced ductility of bimodal Al alloy, proposed by Tellkamp et al. [24]. Cracks propagate through the brittle FG region, but are blunted by large, ductile coarse grains.

In the case of bimodal grain distribution calculating the average grain boundary strengthening can be complex. Therefore rule of mixture can be taken under consideration to state an average grain size:

$$D = (f_{CG} \times d_{CG}) + (f_{FG} \times d_{FG}) \qquad (8)$$

Where d_{CG} and d_{FG} represent the average grain size of CG and FG regions, respectively and f_{CG} and f_{FG} represent the area fraction of CG and FG regions, respectively [30].

Another interesting way to increase ductility is believed to be by tailoring the Grain Boundary Misorientation Angles (GBMA) [26–28]. It is known that High Angle Grain Boundaries (HAGB) that have grain boundary misorientation angle (GBMA) larger than 15° provide effective barriers to dislocation movements, but also against dynamic recrystallization and grain growth by cyclic deformation. Dislocations are effectively locked into grain as they cannot pass to neighbouring grains across HAGB, leading to preservation of high strength. At the same time, Low Angle Grain Boundaries (LAGBs) cannot restrict the movement of mobile dislocations over grain boundary, ultimately leading to increased ductility [27, 28].

1.5 Objectives of the study

The main objectives of the study are to gain deeper understanding of microstructural aspects for high mechanical strength – high ductility nano MMCs; and consequently develop processing parameters to obtain optimised microstructure (and composition) of the composite. In order to accomplish simultaneous strength and ductility, several optimisation steps need to be taken under consideration.

The main goals are:

- Tailor strength and ductility of nanoparticulate reinforced aluminium alloys by increasing strength with retained ductility.
- Describe impact of microstructure related features (nanoparticle dispersion and content, angle of grain boundaries, grain size, effect of bimodal structure etc.), on mechanical properties of the MMCs.
- Assessment and quantification of strengthening mechanisms.
- Produce high strength MMC with minimal processing steps.

These goals are going to be reached by optimising:

- The preparation of blends
    - Milling parameters
    - Reinforcement content
    - The content and type of PCA
- Compaction of milled blends

Throughout the thesis, following technological and scientific aspects will be addressed:

- Mechanical milling of MMC blends
- Compaction of milled blends
- Microstructural characterisation of blends and bulks
- Mechanical testing of blends and bulks
- Assessment of strengthening mechanisms

2. MATERIALS AND EXPERIMENTAL METHODS

2.1 Starting materials

Aluminium alloys

Pure Al-powder provided by ECKA Atomized Aluminium Powder Co had a purity level of 99.5% [DIN EN 576] and a mean particle size smaller than 63 µm (Fig. 3A). The 6061 alloy (AlMg1SiCu) with mean particle size under 45 µm, was provided by TLS Technik GmbH & Co. (Fig. 3B). The AlMg5 alloy (Al5019) provided by ECKA Atomized Aluminium Powder Co possessed a mean particle size smaller than 63 µm (Fig. 3C). The S790 (experimental 7xxx series) alloy (AlZn11Mg2Cu) (Fig. 3D) as well as the S250 (experimental 4xxx series) alloy (AlSi20Fe5Ni2) (Fig.3E) were all provided by Peak Werkstoff GmbH.

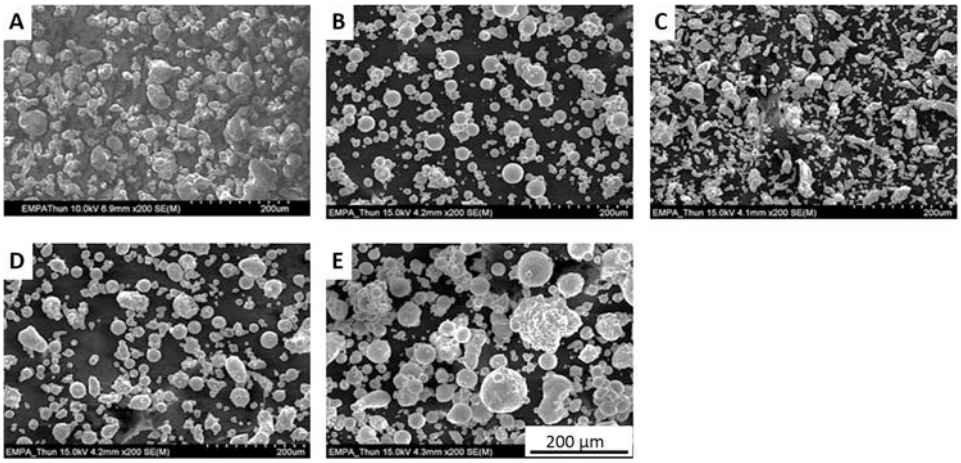

Figure 3. Raw matrix materials: A) Aluminum pure; B) AL6061; C) AlMg5; D) S790; E) S250.

Carbon based reinforcements

6 different carbon nanotubes or fibres were used as carbon based reinforcements (Fig. 4A-4D) and are referred here as CNT. For all these CNTs, an average density of 1.8 g cm^{-3} was assumed for calculations. The CNTs were chosen to have different properties. Therefore highly agglomerated Baytubes (Fig.4A), agglomerated EPFL CNTs in raw and recrystallized state (Fig. 4B), highly ordered CEA CNTs in raw and recrystallized state (Fig. 4C) slightly agglomerated carbon fibres (VGCF) with larger outer diameter of 110 nm (Fig. 4D) were chosen. Other properties are described in Table 1 while their morphology is presented in Fig. 4.

Table 1. CNTs used as a reinforcement [31].

Name	Mean outer diameter [nm]	Length [µm]	Producer / comments
Baytubes	13-16	1-10	Bayer Material Science GmbH, Germany. Agglomerates of 0.1-1 mm [32]
EPFL raw	11		Ecole Polytechnique Fédérale de Lausanne, Switzerland. [33], [34]
EPFL Recrystallized	11		Heat treated 1700-2000 °C [33], [34]
VGCF	110	20	Hodogaya chemical, Japan
CEA raw	55	250-850	Commissariat à l'Energie Atomique et aux Energies Alternative, France. [35]
CEA Recrystallized	55	250-850	Heat treated 1000 °C for 2h [36]

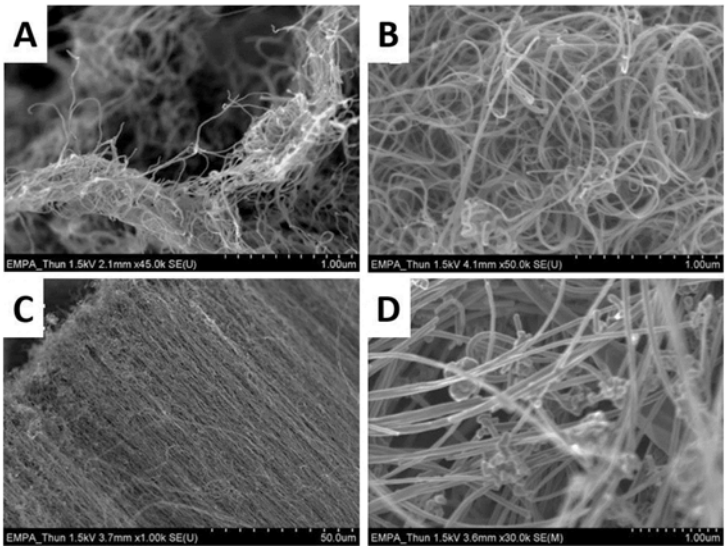

Figure 4. Carbon based reinforcements used: A) Baytubes; B) EPFL raw; C) CEA raw; D) VGCF. Morphology of heat treated CEA and VGCF CNTs are similar to their raw precursors and are therefore not presented [31].

Oxide based reinforcement

Aeroxide Alu65 γ-Al_2O_3 nanoparticles supplied by Evonik Industries were used as oxide based reinforcement. Alumina nanoparticles had a BET surface area of 65 m^2/g, corresponding to mean equivalent particle size of 23 nm, assuming spherical particle morphology (Fig. 5).

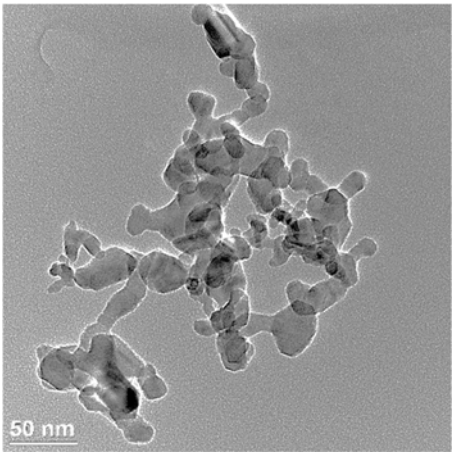

Figure 5. TEM micrograph of Aeroxide® Alu65 Al_2O_3 nanoparticles [37].

2.2 Materials processing

The metal matrix powders were mixed with the CNT reinforcement in a 250 ml stainless steel vial using a Retsch PM400 planetary ball mill at 360 rpm under Ar atmosphere varying the milling time from 1 to 20 hours. As PCA) 1.5 wt% stearic acid (SA) was used in all cases except for Baytubes CNTs where 15 wt% of heptane was used to avoid excessive cold welding. 100Cr6 hardened steel balls with a diameter of 10 mm were used as milling media with a BPR of 10:1 [31, 38].The main milling parameters had been selected based on a previous work dealing with the dispersion of silicon carbide nanoparticles into aluminium matrix by Kollo et al. [7] as well as [38].

For dispersing oxide reinforcement into AlMg5 metal matrix, Retch PM400 but also a prototype cube mill (P&S Powder and Surface GmbH, Germany) was used. In conventional commercial planetary ball mill, the cylindrical milling vessels create shearing forces upon ball impacts. While in experimental cube mill, the planet-like movement is incorporated with cube shaped milling vessels, leading to flat impact forces exceeding the energy provided by cylindrical vessel (Fig. 6) [37].

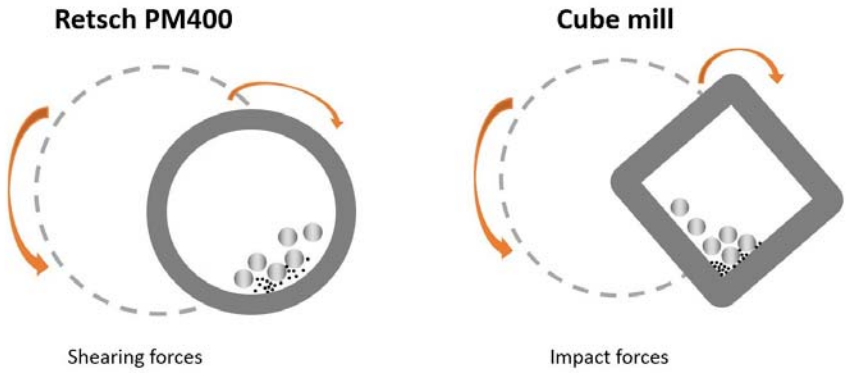

Figure 6. Schematic of milling vessels of commercially available Retsch PM400 planetary ball mill and prototype cube mill.

The AlMg5 powder was mixed with Al_2O_3 nanoparticles with different volume fractions. During the initial study, milling was conducted with PM400 using similar milling parameters as CNT reinforced MMCs with additional optimisation of PCA and milling duration. In the study of cube milling, the content of reinforcement was thoroughly investigated and the abbreviations are used in the manuscript, as shown in Table 2. Planetary ball-milling with a cube shaped milling vessel was used at 350 rpm under Ar atmosphere with milling period up to three hours. Hardened stainless steel milling vessel and 100Cr6 hardened steel balls with a diameter of 10 mm were used as milling media with a BPR of 10:1. SA was used as a PCA and its content was adapted to the content of surface area of nanoparticles (Table 2) [37].

Table 2. The compositions milled with cube mill [37].

Composition	Al_2O_3 reinforcement [vol%]	Stearic acid [wt%]
A_un (unmilled)	-	-
A_m (milled)	-	0.30
A-0.2np	0.20	0.30
A-0.3np	0.30	0.46
A-0.4np	0.40	0.61
A-0.5np	0.50	0.75
A-1.0np	1.00	1.50

The milled powders were collected and handled in a glove-box under Ar (O_2 < 100 ppm, H_2O < 150 ppm) where they were passivated before being used for consolidation.

Uniaxial hot pressing

Uniaxial hot pressing was conducted under air atmosphere with 200 Ton uniaxial press (Walter + Bai AG, Switzerland). Following uniaxial hot compaction techniques were used;

First technique (technique 1) by using 30 mm diameter steel moulds for compacting with 570 MPa at preheating temperatures of 350 °C or 450 °C with dwell time of one hour. This technique yielded to round sample with thickness of 6 mm and diameter of 30 mm [38].

Second and more advanced technique (technique 2) included using the square steel moulds with the size 55x55 mm. The moulds were heated with 3 °C/min under primary vacuum (1 mbar) and held at 350 °C for 14 h to induce drying and degassing of the powder blend followed with 1.5 hours at 550 °C [39]. The moulds were then flushed with Ar in furnace and transferred rapidly (less than 5 seconds) under the press for compaction to produce the bulk samples with dimensions of 55 x 55 x 7 mm. The samples were naturally cooled in air. The temperature profile used in this compaction technique will hereinafter be considered as Compaction Heating Cycle (CHC). [31, 37].

Forge compaction

Hot forging was conducted to directly compact milled Al-MMC powders. The powders were inserted into s235 steel capsules (d = 25 mm, L = 70 mm) in glovebox under Ar (O_2 < 100 ppm, H_2O < 150 ppm) after which the capsules were closed with valve and removed from glovebox. The capsules were then evacuated to $1x10^{-5}$ mbar and similar heating cycle as CHC was performed to the vacuumed capsule to induce degassing. After degassing, capsule was compacted under 500 Ton uniaxial press (MKH Press, Finland). If the capsule had broken, the sample was discarded, if not then the sample was reheated and re-forged 4 times to achieve full density. The samples were naturally cooled after which the capsule was removed and UTS dog-bone samples were machined perpendicular to forging direction.

Spark plasma sintering

Spark plasma sintering (SPS) was carried out using FCT SPS HPD 10 machine (FCT Germany). Approximately 26 g of powder was loaded into a graphite die with 50 mm diameter. For easy removal of the sintered pellet, the graphite die was isolated from powder with graphite paper. A uniaxial pressure of 50 MPa was applied throughout the process. Sintering was conducted under primary vacuum, with the heating rate of 100 °C/min. Changes in temperature, average intensity and voltage of the pulsed current and sintering displacement were recorded in-situ by a computer during the entire sintering process. All the compositions were sintered at 550 °C, with a dwell time of 15 min followed by natural cooling in furnace [30].

Hot isostatic pressing

Hot isostatic pressing was conducted on capsules that were filled with Al-MMC powder in the same way as for forge compaction. The capsules were evacuated and welded shut. The HIP was carried out using AIP HP630 at 550 °C under 100 MPa Ar overpressure with dwell time of 60 min. Capsules were removed and UTS samples machined lengthwise of capsule.

2.3 Methods of characterisation

The morphology of the powders was characterised using a Zeiss Axiopan optical microscope and CFE-SEM (Hitachi S-4800). The carbon structure in the raw CNTs, the blends and the bulks were investigated by Raman spectroscopy (Renishaw invia) at 514 nm with 12.4 mW. At least 10 Raman measurements per sample were conducted. The spectra were deconvoluted, fitted and the integrated intensity ratio of the D- and G-band of carbon (I_D/I_G) was calculated. The hardness was measured with a MHT-4 Vickers microhardness tester using a load of 0.15 N for 15 s. Vickers macrohardness measurements were made according to EN ISO 6507-1 with a load of 20 kg for 15 s (220, GNHEM Härteprüfer AG). At least six measurements were performed on polished surface of each sample. Differential Thermal Analyses (DTA) were conducted with a Netzsch STA C409 under 50 ml/min Ar flow. The bulks were characterised with CFE-SEM (Hitachi S-4800) as well as with HR-TEM (Jeol JEM-2200FS TEM/STEM). TEM samples were prepared with an Allied multiprep polishing system and ion milled using a Fischione Instruments TEM Mill 1050. Electron Backscatter Diffraction (EBSD) and Transmission Kikuchi Diffraction (TKD) were measured with a TESCAN Lyra3 FE-SEM and an AMETEK EBSD, respectively. Samples for EBSD mapping were prepared with a Leica EM-TIC 3x ion polisher/cross sectioner. The grain size was estimated by measuring and averaging the length and width of grains using ImageJ® image analysis software. Conventional EBSD was used to reveal CG regions as well as area fraction of FG/CG regions while TKD and TEM were used to reveal the morphology of fine grains in FG regions. The average of at least five regions containing over 300 grains was taken into account while calculating the average grain size and the area fractions of FG/CG. The crystallite structure was investigated using Synchrotron radiation at a wavelength of 0.66 Å with 18.8 KeV at the Paul Scherrer Institute (PSI, CH). The crystallite size was calculated using the Scherrer equation from Al[111] peak measured with a BRUKER Discovery D8 with Cu Kα (λ = 1.5148 Å, 40 kV and 40 mA) in the 2θ range 30-120 ° using a linear detector. The instrumental broadening was determined with a α-Al_2O_3 standard. Elemental oxygen and carbon contents were measured using an ELTRA ONH2000 infrared cell. Flat bone-shaped tensile specimens with a thickness of 4 mm, gauge length of 12 mm and a distance between shoulders of 26 mm, were machined from flat 55 x 55 x 7 mm square plates in case of hot pressed samples or from 6 mm thick round samples (D = 50

mm) or from 40 x 70 x 7 mm flat samples in the case of hot forging and HIP. The tensile specimens were always prepared perpendicularly to the pressing direction and the tensile tests were carried out at room temperature using a universal testing machine (Hug Maschinenfabrik AG) with the speed of 1 mm/min. For the density of the bulk samples, the Archimedes method according to ISO 3369:1975 was used.

3. DEVELOPMENT OF Al-MMC

3.1 Study of matrix alloys

Four commercially available aluminium alloys were chosen to evaluate the influence of CNT reinforcement on different aluminium alloys [38]. The results are compared to the previous study performed in our group on pure aluminium matrices [12]. All the alloys were milled (Retsch PM 400) and compacted under similar conditions (technique 1 – see chapter 2.2) that proved to be adequate for achieving dense bulk material. Indeed, all the samples possessed a density higher than 92% of the theoretical density. In Figure 7A hardness changes can be observed as a function of the reinforcement weight fraction.

The highest hardness increase was observed with Al6061. Fivefold increase in hardness was obtained when adding only 3 wt% of Baytube CNTs, reaching 230 HV20 compared to about 40 to 50 HV20 for the unreinforced annealed alloy. Further increasing the reinforcement content did not lead to higher mechanical properties of the MMC, and the density even slightly decreased. Therefore for Al6061, a maximum amount of 3 wt% CNTs could be successfully dispersed. Fourfold hardness increase was noted with AlMg5 alloy based MMCs and the hardness increased up to 260 HV20. The highest hardness of the study was achieved with the S250 alloy reaching up to 390 HV20 for 6 wt% CNT reinforcement. However the starting alloy having already 175 HV20, so the growth factor of hardness was the lowest (Fig. 7A). Among the investigated parameters, the MMCs produced with AlMg5 and Al6061 matrices possessed highest hardness with 3 wt% CNT reinforcement. Using higher content led to decrease of hardness up to 6% and 14% as compared to maximum values in the case of Al6061 and AlMg5 respectively. With composites based on S250 and S790 matrices the hardness decrease for 9 wt% CNT was more evident being 22% and 35% lower than the maximum values respectively.

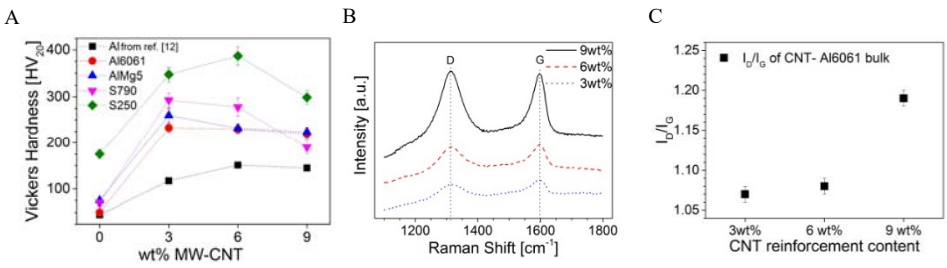

Figure 7. A) Hardness of MW-CNT reinforced Aluminum alloys. B) Raman Spectra of Al6061 matrix MMCs. C) Intensity ratio ID/IG of Al6061 matrix MMCs [38].

All four alloys could be reinforced with CNTs leading to significant hardness increases. However, in order to focus the study only one widely used and investigated alloy, the Al6061 was further investigated as matrix material.

The hot pressed CNT-Al6061 bulks were investigated by Raman spectroscopy. Typical spectra for the Al6061 composites can be seen in Fig. 7B. The spectra show two distinctive bands D (Disordered) and G (Graphite) at 1310 cm^{-1} and 1597 cm^{-1} respectively. The D-band seems to increase with the CNT content indicating a higher content of damaged CNTs. This is confirmed by the evolution of the integrated intensity ratio between the D and G-band in Fig. 7C. The I_D/I_G ratio increases with increasing CNT content especially at the highest investigated CNT content, i.e. 9 wt% .

In the following, the influence of the hot pressing temperature was investigated. Thus the increase of the compaction temperature from 350 °C to 450 °C resulted in higher hardness and density of the MMCs (Fig. 8A). However, using 450 °C induced the formation of aluminium carbide (Al_4C_3) as shown in Fig.8B. No Al_4C_3 could be identified by XRD directly after milling.

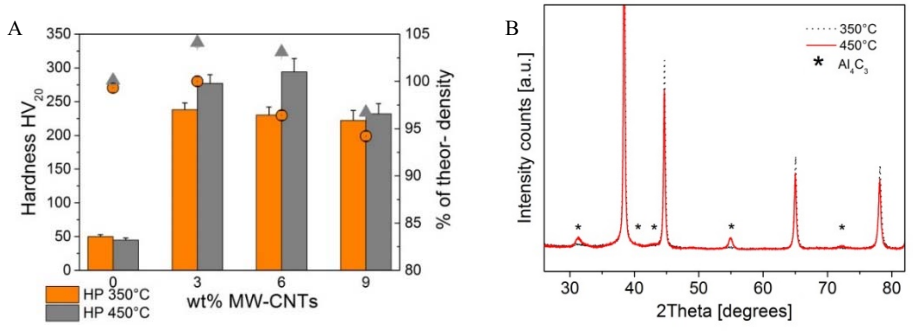

Figure 8. A) Influence of compaction temperature on hardness and density of Al6061 based MMCs. B) XRD indicating aluminium carbide (Al_4C_3) formation on 6 wt% CNT reinforced Al6061 MMC after increasing compaction temperature to 450 °C [38].

The 6xxx series alloys are normally heat treated to improve their mechanical performances. Thus standard heat treatments T4, T6 and T5 were performed on the investigated Al6061 matrix nanocomposites. Figure 9A describes the hardness response after these heat treatments. No noticeable increase was observed for composites. On the contrary, for 3 and 6 wt% CNT, the heat treatments (T4 and T6) led to even a decrease of the composite hardness. For 9 wt% CNT, the hardness was not influenced by none of the used heat treatments. Furthermore, the relatively high temperature used during solution phase heat treatment (T4 and T6) seemed to contribute to the formation of Al_4C_3 (Fig. 9B).

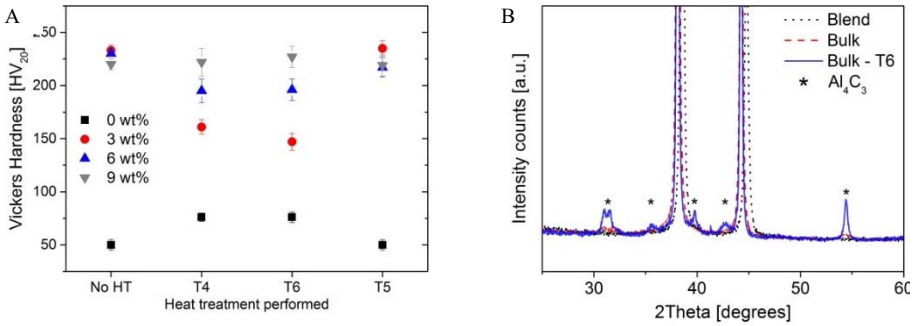

Figure 9. A) Hardness of Al6061 matrix MMCs regarding different heat treatments. B) XRD pattern of 3 wt% CNT reinforced Al6061 depending on different heat treatments [38].

Rietveld refinement was performed to assess the crystallite size of heat treated CNT-Al6061 MMCs. For solution phase heat treatments only T6 will be presented as there was no significant difference on crystallite size between T4 and T6 treatments. The crystallite size increased while using high temperature solution phase heat treatment for all the reinforcement quantities (Fig. 10).

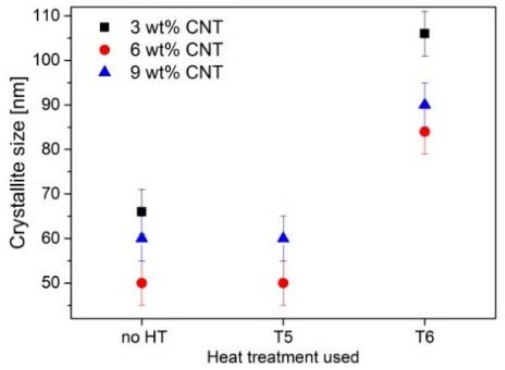

Figure 10. Calculated crystallite size of Al6061 matrix CNT composite with different heat treatments used [38].

Discussion

Mechanical milling was used to disperse high quantities (3, 6, 9 wt%) of MW-CNTs into 4 different aluminium alloys to continue previous work on similar contents of CNTs in pure aluminium matrix by Bradbury et al. [12]. High hardness values and capability of dispersing up to 9 wt% CNTs into aluminium matrix was achieved by the authors. The macro hardness of the Al-6 wt% CNT composite increased more than threefold compared to the unreinforced aluminium bulk compacted under the same conditions. A further increase of the CNT content up to 9 wt% did not lead to higher hardness, on the contrary the hardness had decreased.

Similar trend was noted with all the investigated aluminium alloys in this present study. All the alloys that were milled and compacted under similar conditions produced dense bulk samples and their hardness increased by a factor of 2 to 5 compared to the respective pure unmilled alloy. The highest hardness increase was achieved with the Al6061 based composite with only 3 wt% CNTs reaching the hardness up to 230 HV20 that is fivefold over the unmilled alloy (Fig. 7A).

Relatively high Disorder peaks seen on Raman spectra (Fig. 7B) and the increase of the I_D/I_G ratio (Fig. 7C) indicate that CNTs were damaged by the high energy ball impacts during processing. Higher content of CNTs will lead to more damaged CNTs on the blend. On the opposite, Bradbury et al. [12] showed the the I_D/I_G intensity ratio being almost constant for CNT content between 3 and 9 wt% in pure aluminium. Authors then suggested that the CNTs are being covered by the soft aluminium matrix protective layer during milling and thus protecting the CNTs from further damages as also described by Choi et al. [40]. In present work, the raw alloys are significantly harder than pure aluminium and the coverage of the CNT should take longer, meaning raw CNTs are subjected for a longer time to direct ball impacts.

Three alloys Al6061, AlMg5 and S790 (7xxx) possessed their highest hardness for 3 wt% CNTs. At higher CNT concentrations, the hardness slightly decreased. For the S250 (4xxx) alloy, the highest hardness was obtained with 6 wt% CNTs (390 HV20), as in the case of pure aluminium matrices [10]. However for higher CNT contents in the S250 alloy, a considerable decrease in hardness was observed while in the case of pure aluminium the hardness did not decrease so much for 9 wt% CNT. This could be due to insufficient milling energy for dispersing high content of CNT into S250-s hard matrix.

In order to optimise the hot pressing parameters, higher compacting temperature was investigated with the Al6061 matrix. Increase in hardness and density of MMCs was noticed with the increasing compaction temperature from 350 to 450 °C (Fig. 8A). However 450 °C induced the formation of Al_4C_3 (Fig. 8B) that could lead to unwanted brittleness or corrosion issues of the produced MMC. Therefore 350 °C was selected as preferred option for CNT reinforced aluminium alloys.

The 6xxx series alloys are normally precipitation heat treated to improve their mechanical performances. However, no hardness improvement was observed after standard heat treatments on our Al6061-CNT composites. Indeed, for lower reinforcement contents (3 wt% and 6 wt%), the hardness even decreased slightly after solution phase heat treatments. For 9 wt% reinforcement, the heat treatments had no notable influence on the hardness of composites. The crystallite size of matrix increased after T4 and T6 treatments (treatment temperature is 530 °C. Considering the grain growth effect on Hall-Petch strengthening, it is not surprising that the hardness decreases after the heat treatments. For high CNT concentration, i.e. 9 wt%, even if the crystallite size increases after T4 and T6, the hardness remains constant. No explanation could be proposed so far and further investigations, especially structural characterizations are necessary. The lower temperature artificial aging (T5) did not induce any change neither of the crystallite size nor of the hardness whatever the reinforcement fractions (Fg.10A).

Conclusion

To conclude the study on CNT reinforced different aluminium alloys main points are brought out. In order to improve hardness of aluminium alloys, high content of MW-CNTs were successfully dispersed in 4 different aluminum alloys by high energy planetary ball milling. The resulting composites were 3 to 5 times harder than the pure alloy compacted under same conditions.

The hot pressing temperature was optimized. The higher pressing temperature of 450 °C led to higher hardness and density of MMC but also enhanced the formation of Al_4C_3. Therefore 350 °C was proposed for direct uniaxial hot pressing.

The standard heat treatments (T4, T5, and T6) performed typically on Al6061 were found to have no positive influence on the hardness of the investigated nanocomposites. On the contrary in the case of 3 wt% and 6 wt% reinforcement the hardness decreased after solution phase heat treatments (T4 and T6) possibly due to crystallite size growth induced by elevated temperature. For 9 wt%, the hardness remained at a high level after the high temperature treatments even after crystallite size had increased.

This study demonstrated the effective ways to greatly increase hardness of materials. To further tailor the properties of material, second study was conducted to investigate the effect of different CNTs on single alloy matrix. As heat treatment led to no improvement of MMC, the non-heat treatable AlMg5 was chosen for the next study.

3.2 Study of reinforcements

To focus on the influence of the added nano-reinforcement particles and to remove the effect of heat treatments, the AlMg5 alloy was chosen as matrix [31].

3.2.1 CNT reinforced MMCs

Powder blends of different CNT-MMCs

Six CNTs with different morphologies (Fig. 4 and Table 1) were used to reinforce AlMg5 alloy matrix. The study was conducted to investigate the effect of CNT morphology (agglomerated or ordered), size (outer shell diameter and length of the fibre) and the reinforcement content. The pristine CNTs were characterized with Raman spectroscopy. All the raw CNTs show the distinctive G (Graphite) and D (Disordered) bands at 1340 cm^{-1} and 1570 cm^{-1} respectively (Fig. 11A). The integrated intensity ratio between these two bands I_D/I_G was between 0.1 and 1.2 (Fig. 11B) giving a relative information on the CNT quality. Larger ratio would indicate higher number of defects and therefore lower quality of CNT. Among the investigated raw CNTs, the Baytubes seem to have the largest number of defects while the VGCF seem to have the fewest defects [31].

Initially AlMg5 matrix was milled with 1 vol% of all the CNTs for 6 hours to recognize any differences in reinforcement capabilities. After 6h of high energy ball milling, the I_D/I_G drastically increased and was in the range from 2.3 to 3.6 indicating an increase of disorder for all the blends. Nevertheless the Graphite band was still present. Blends reinforced with CEA raw CNTs and VGCF had the highest ratio values whereas blend reinforced with EPFL CNT had the lowest value. However, there seem to be no direct correlation between the ratio before and after milling [31].

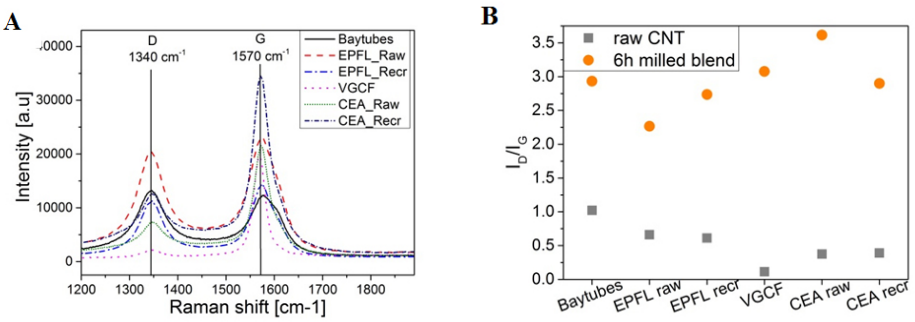

Figure 11. A) Raman spectra showing the G- and D-band of the carbon nanotubes in the raw starting CNTs. B) Typical I_D/I_G ratio for the investigated raw CNTs and 1 vol% CNT blends after 6h of high energy milling [31]. Measurement uncertainty is counted, but the error bars are too small for visibility.

All the 1 vol% CNT reinforced powder blends had equiaxial morphology with particle sizes ranging from 30 to 50 µm after 6h of high energy ball milling with Retsch PM400. All the powders possessed a micro-hardness around 200 HV0.15 (Fig. 12A), about 4 times higher than the non-milled starting alloy (50 HV0.15). The blends made out of the EPFL recrystallized CNTs were in the same range as unreinforced milled AlMg5 alloy particles and about 100 HV less than the other blends. Due to the size of the powders relative to the indent print, the hardness values are highly dispersed. The crystallite size of the powders and bulks is plotted in Figure 12B. The raw non-milled alloy had an Al [111] crystallite size around 85 nm. During milling, even without any CNTs, the crystallite size of the starting alloy decreased to 50 nm. A further decrease is observed with the addition of CNTs with sizes between 30 and 36 nm. These trends are still observed after hot compaction. Even if the crystallite size increased after the high temperature process (CHC), all the composite materials exhibited an average crystallite size between 74 and 91 nm while the non-reinforced alloys had Al crystallites at 190 and 140 nm for non-milled and milled conditions respectively [31].

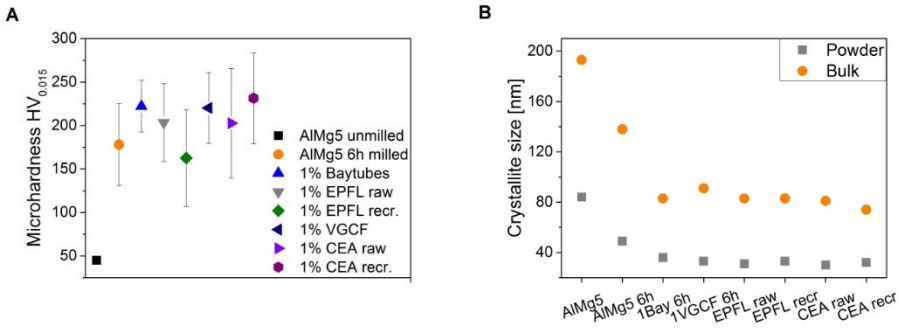

Figure 12. A) Micro hardness of composite powders. B) Al crystallite size of powders and bulks. Standard deviation of measurement was under 1 nm [31]. Error is counted, but error bars are too small for visibility.

Bulk composites

After compaction (CHC) all the bulks had densities from 2.70 to 2.75 $g \cdot cm^{-3}$, meaning higher than the theoretical density (2.64). To verify the origin of higher density, measurements of the oxygen and carbon were measured. The contents in different bulks indicated a content of 1±0.02 wt% of O_2 and 1±0.01 wt% of C whatever the CNT used indicating to slight oxidation during high temperature compaction at 550 °C. The carbon content was concurrent with the added CNT and SA content, meaning no additional carbon was entering during processing.

The hot compacted pure AlMg5 alloy had a hardness around 60 HV20 (Fig. 13) which is in agreement with values typically referenced for this alloy. Milling the pure alloy with stearic acid for 6 h still increased the hardness to 120 HV. The addition of 1 vol% of CNT further improved the hardness and values between 170 and 190 HV20 were measured. This corresponds to a threefold increase compared to the unmilled pure alloy. For comparison, the highest strength commercial 5xxx alloy, AA5083 strain hardened to an extra hard condition (H19) exhibits typically 120 HV20 that is similar to the 6 h milled pure AlMg5 alloy and lower than here developed CNT reinforced AlMg5 composites.

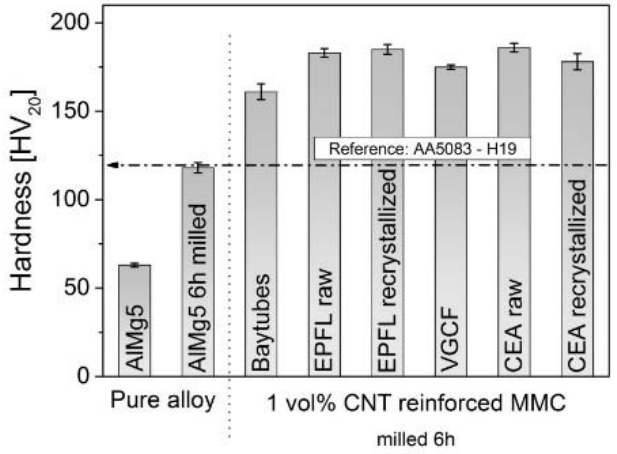

Figure 13. Macro hardness of the compacted materials. The dashed line at 120 HV corresponds to the value reported for an industrial AA5083-H19 for comparison [31].

A similar enhancement was observed for the tensile strength of the materials. Whatever the investigated CNTs, the tensile properties of the composites were in the same range with UTS around 500 to 600 MPa and elongation at rupture around 1%. A representative stress-strain curve of the AlMg5-1 vol% Baytubes is presented in Figure 14 together with the response of the hot compacted pure AlMg5 alloy obtained from raw and milled powders. The hot pressed AlMg5 alloy had an ultimate strength around 200 MPa and an elongation at rupture of 20 to 25%. High energy ball milling increased the UTS by a factor of 2 to 400 MPa. For comparison, the commercially available high strength alloy AA5083 reaches UTS values around 420 MPa but with an elongation at rupture around 5%.

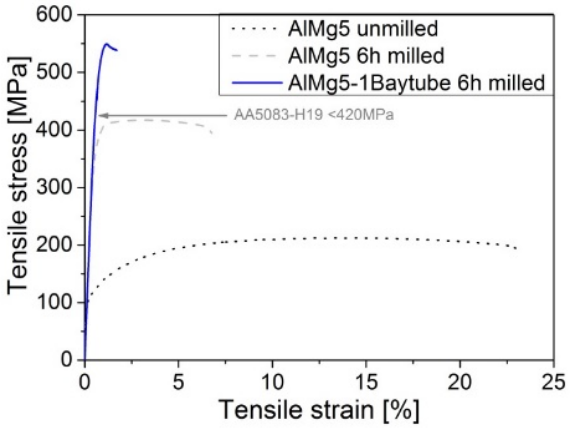

Figure 14. Typical tensile strength-strain curves of different bulk AlMg5 based materials as a function of ball milling and addition of reinforcement [31].

Extensive TEM analyses were performed on the compacted AlMg5-1 vol% CNT composites for giving a representative picture of the composites. At least 6 TEM samples were prepared for each investigated composite to provide sufficient area of investigation. No excessive agglomeration of CNTs could then be observed even for Baytubes that are delivered as highly agglomerated powders. The CNT dispersion is similar to the one presented in Figure 21C for higher carbon nanotube contents. Al_4C_3 structures could be however seen (Fig.15). In Figure 15B, it appears that some aluminium carbide is formed by the partial reaction of CNT with Al as already described in literature [14–17] Moreover, from TEM analyses, it seems that the CNTs were shortened to lengths between 80 and 300 nm. An average grain size of aluminium around 80 to 90 nm could be measured that is in agreement with the crystallite size determined with XRD. No preferential orientation of the CNTs could be observed. Similar random orientations were also reported by Suryanarayana et al. for nanotubes reinforced metal matrix composites [2].

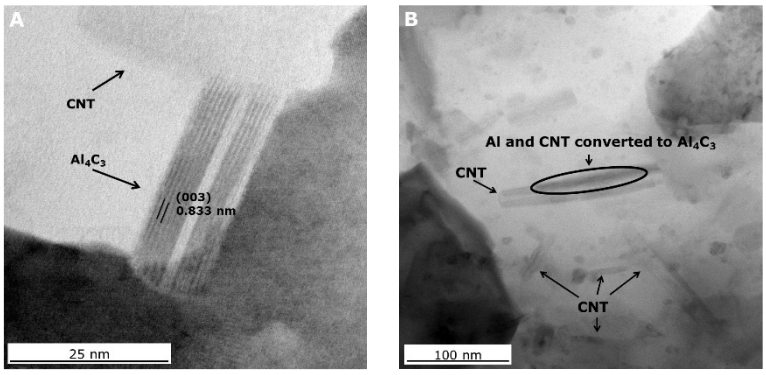

Figure 15. A) Al_4C_3 and CNT visible in MMC B) Partial conversion of Al_4C_3 from CNT [31].

Influence of milling duration

To investigate the effect of milling time the Baytubes CNTs were used as reinforcement with content of 1 vol%. The particles become flattened and larger than the starting AlMg5 powder after 1 h milling (Fig. 16). After 4 h milling, particles achieved equiaxed morphology and the mean particle size becomes similar to the starting powder. Further increasing the milling time, induced a growth by agglomeration of the particles. After 20 h of milling, a very large particle size distribution was observed with small (a few tens of microns) and very large particles, over 200 μm. Under the investigated parameters, the optimum milling duration is ranging from 4 to 6 h (Fig. 16).

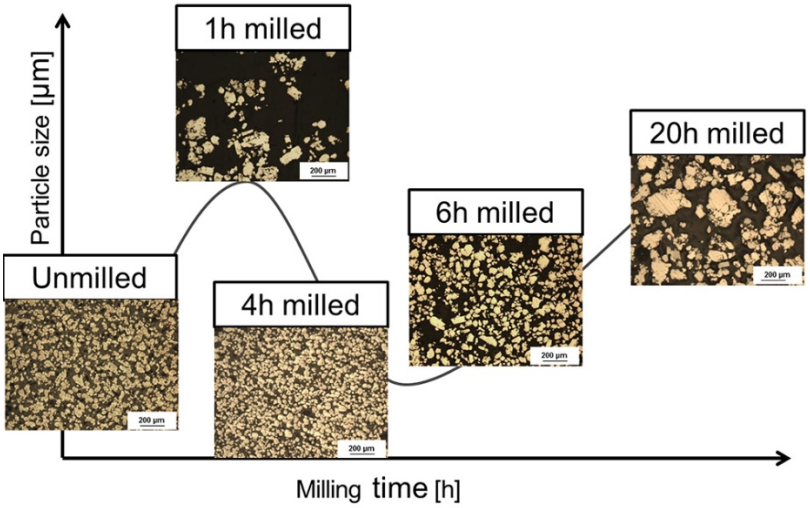

Figure 16. Influence of milling time on the particle size and morphology of the AlMg5–1 vol% Baytubes blends. Scale bars are all 200 μm [31].

The damage of the CNTs during milling can be seen on Figure 17. The Raman spectra measured on the blends shows the evolution of the disorder D peak and graphitic G peak as a function of the milling time (Fig. 17A). The I_D/I_G ratio increases continuously with the milling time (Fig. 17B) indicating damage towards CNTs. Nevertheless the G peak is still existing after 20 h of milling suggesting that there is still CNTs existing in the MMC [31].

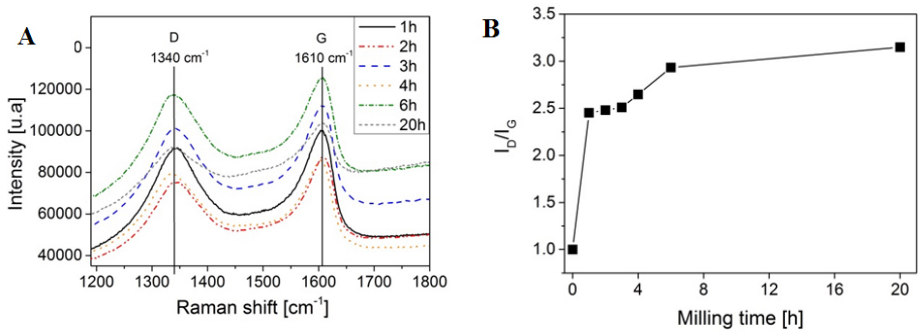

Figure 17. Influence of the milling time of AlMg5-1Vol% Baytube reinforced composite on the G- and D-band (A) and on I_D/I_G (B) [31]. Measurement uncertainty is counted, but error bars are too small for visibility.

The blends compacted with technique 2 had a density ranging from 103 to 104% of theoretical density whatever the milling time used. The bulk macro hardness showed a maximum around 170 HV20 from 2 to 4 h of milling and decreases for longer milling times (Fig. 18). The UTS however reaches a plateau at 500 MPa from 2 to 20 h of milling. The elongation at rupture was around 1% for all the investigated milling times. In the case of 20 h, only 1 tensile specimen out of 3 could be successfully tested due to early brittle rupture between the tensile machine grips.

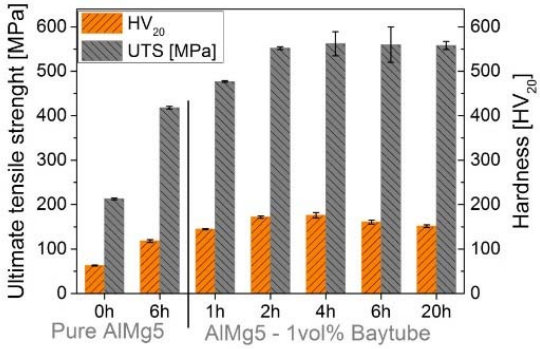

Figure 18. Influence of milling time on hardness and ultimate tensile strength of bulk composites [31].

Influence of the CNT content.

To further investigate the influence of the agglomeration state of the starting material on its dispersion by milling, two types of CNTs were selected: the VGCF as less agglomerated large diameter CNTs and the Baytubes as highly agglomerated smaller diameter CNTs. The content of reinforcement material was increased from 1 to 5 vol%. The milling time was varied from 1 to 20 h and the other processing parameters were kept constant.

After 1 h of milling the blend made out of VGCF CNTs had a flake-like morphology (Fig. 19). Homogeneous particle size distribution of roughly 35 µm is achieved after 10 h of milling. Increasing milling time to 20 h leads to a mean particle size growth up to about 70 µm. For the highly agglomerated Baytubes CNTs, the powder morphology evolution is similar to the VGCF-based blends.

The measured density of the compacted composite bulks was in any case slightly over 100% of theoretical density regardless of which reinforcement was used. The oxygen content of the bulks was measured around 1 wt% while the carbon content reached around 4.6 wt%. With higher CNT MMCs, the more aluminium carbide is expected to form, compared to the composites reinforced with only 1 wt% of CNT.

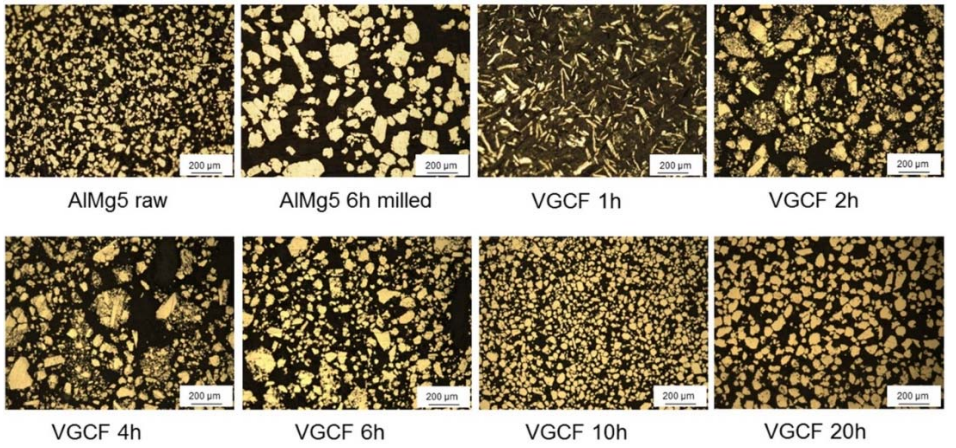

Figure 19. Evolution of powder morphology of AlMg5-5 vol% VGCF blends compared to the pure alloy powder as a function of milling time [31].

The ultimate tensile strength of composites was differing noticeably regarding the milling time. The UTS of the composites reinforced with 5 vol% VGCF increased with milling time, reaching a maximum after 4 to 6 h at about 500 MPa and then decreased. In the case of 5 vol% Baytube reinforced composites however, the UTS had a maximum of 400 to 450 MPa after 1 to 2 h of milling. After 4 h of milling the UTS was decreased to about 280 MPa and increased slightly again after 20 h of milling but reached only about 380 MPa. In all the cases, the elongation at rupture was below 1%, being lower than in the case of 1 vol% of CNT

reinforcement. Moreover the modest UTS values could be attributed to very low ductility of materials as among the three tensile specimens tested, often one or even two of them broke without reaching a plastic deformation zone. The composites reinforced with 5 vol% CNTs are very brittle.

In terms of hardness, for both types of CNTs, the hardness increased with the milling time and seems to level off at similar values around 260 HV after 6 to 10 h of milling. It is worth to note that the 1 h milled flake-like powder observed in blends made with VGCF (Fig. 19) resulted in the lowest bulk hardness values, being even softer than pure AlMg5 alloy (Fig. 20A).

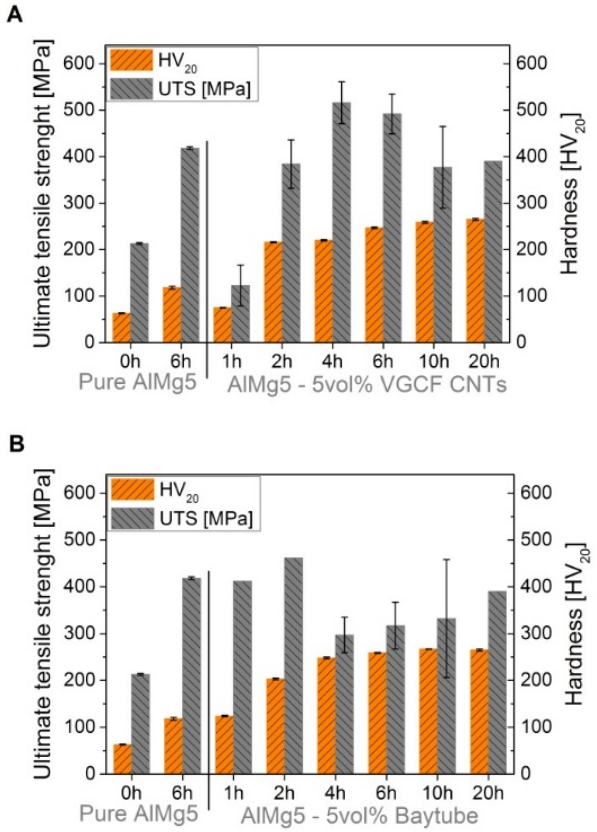

Figure 20. A) Hardness and UTS of 5 vol% VGCF reinforced composite compared to the pure AlMg5 alloy. B) Hardness and UTS of 5 vol% Baytube CNT reinforced composite compared to the pure AlMg5 alloy [31].

Compared to 1 vol% reinforcement, the composites reinforced with 5 vol% seemed to be have more CNT agglomerations as discovered by STEM (Fig. 21A,B). However, regarding the dispersion of the Baytubes and the VGCF in the

composites, no significant differences can be seen. The global CNT reinforcement distribution can be considered homogeneous (Fig.21C).

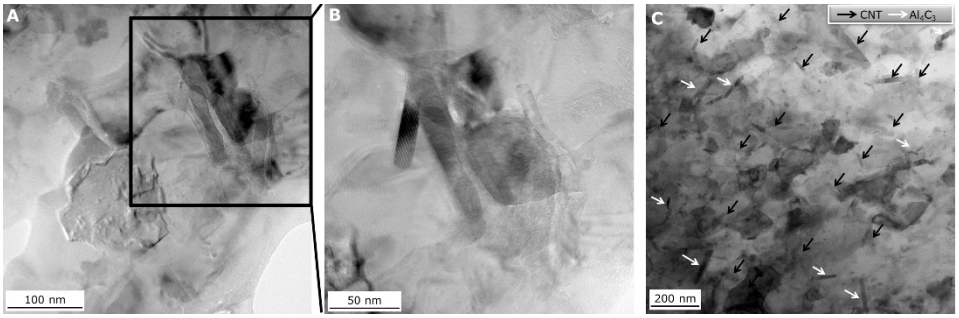

Figure 21. A,B) Agglomeration in 5 vol% Baytube reinforced composite. C) Al_4C_3 and CNT distribution in 5 vol% VGCF reinforced composite [31].

As higher reinforcement content led to highly brittle and thus unfavourable material for structural applications, lower amount of reinforcement was then investigated. Thus 0.5 vol% of Baytubes was dispersed in AlMg5 alloy through high energy milling for 6 h. The resulting blends were equiaxed and homogeneous with a mean particle size around 50 μm.

The tensile strength of the bulk AlMg5-0.5 vol% Baytube composites was the highest achieved (Table 3). Indeed 720 MPa could be achieved; however, no improvement regarding the ductility could be measured.

Table 3. Properties of Baytubes reinforced AlMg5 composites [31].

Composition	Hardness HV20	UTS [MPa]	YS [MPa]	Young's modulus [GPa]	Elongation [%]
AlMg5 unmilled	60 ± 0	215 ± 5	115 ± 5	84	21 ± 2
AlMg5 6h milled	120 ± 3	417 ± 8	370 ± 5	86	5.5 ± 0.8
AlMg5 – 0.5 vol% CNT	**200 ± 2**	**723 ± 15**	**644 ± 8**	**90**	**1 ± 0.2**
AlMg5 – 1 vol% CNT	165 ± 2	555 ± 5	500 ± 3	86	1.2 ± 0.5
AlMg5 – 5 vol% CNT	203 ± 2	460 ± x	456 ± x	80	0.2 ± x

x – 2 out of 3 tensile samples broke between the grips due to extreme brittleness.

Discussion

After optimising process parameters, high hardness and UTS could be obtained to AlMg5 alloy reinforced with CNTs. Indeed, the hardness increases up from 60 to 200 HV and a tensile strength around 720 MPa could be achieved with only 0.5 vol% of CNTs dispersed in the AlMg5 matrix. Similar strength has been

reported by other authors after dispersing 5 vol% of B_4C nanoparticles into a very similar 5083 Al-alloy [41]. But to reach a tensile strength of 755 MPa, the authors had to use a more complicated processing procedure involving cryomilling, hi-vacuum degassing and hot isostatic pressing (HIP) followed by extrusion. In current study, authors achieved similar mechanical properties with a considerably simpler processing technique. The mechanical strength achieved is 2 to 3 times above the highest values reported for commercial 5xxx alloys even after extensive work hardening processing steps.

From the mechanical strength of the material and the microscopy analyses, it appears that the used high energy ball milling process enabled to disperse effectively dry CNTs into the Al-alloy matrix without any pre-treatment or functionalization. Furthermore, the nature as well as the initial agglomeration state of the CNTs did not play a key role in the mechanical response of the nano-reinforced composites. Indeed, similar mechanical properties could be achieved for blends obtained using highly agglomerated Baytubes as well as CNTs that were mostly ordered and not agglomerated. This could be explained by the effect of the milling media impacts on the CNTs. The shocks between the powders and the balls induced shortening of the CNTs, leading to a de-agglomeration. The shortened CNTs were then easily dispersed into the soft matrix. The shortening and damaging of CNTs during the milling process have been already reported by other authors [13, 40]. Besides the dispersion of reinforcement, the high energy milling had another important effect for the composites strengthening. The crystallite size of the aluminium matrix was decreased significantly by work hardening and reached a similar value for all the CNTs investigated. Considering the grain-size refinement strengthening mechanism (Hall-Petch effect) [12, 21], it is not surprizing that the strength of the AlMg5-CNT composites were enhanced by a factor of 2 to 3. Strengthening mechanisms are further described in the paragraph 3.4. High energy milling itself already decreased the crystallite size of the matrix by a factor of two and the addition of CNTs further induced a decrease of the Al-crystallites. The temperature during hot compaction process obviously lead to an increase of the crystallites but the growth was more limited with reinforced materials. This could be due to the pinning effect of the nanomaterial at the crystallite boundaries as reported by some authors [42]. The high brittleness of materials was still the problem to be solved. Compared to previous study, the samples could already be tensile tested (during previous study samples were too brittle for UTS tests), but the fracture at rupture was still around 1 to 2% being still not enough for industrial applications.

The milling duration was investigated and the competition between cold welding and fracturing during ball milling was clearly observed. First the soft aluminium alloy powder was flattened and starting to cold weld leading to particle growth. After reaching a certain work hardening induced by the ball impacts, the particles started to fracture. This is a well-known procedure of ductile-brittle milling procedure [6]. In this study we could further observe that the powders started to

agglomerate again after longer milling durations but this did not affect the mechanical performances of the composites. The fact that short milling times lead to a poor mechanical strength could be explained by the combination of flaky shapes, softer particles and heterogeneous CNT dispersion. Liu et al. had also reported that short milling time or low milling energies lead to a covering of the aluminium particles with CNTs and longer times (higher energy) are required to embed the CNTs into the matrix particles [13].

The efficiency of the investigated milling parameters were however limited to low CNT contents. Indeed at 5 vol% of CNT, some clusters could be observed and several tensile specimen broke earlier than others. The composites were then highly brittle. This has been also reported by Esawi et al. [43]. Typically values between 1 and 5 vol% of CNT reinforcement are reported in the literature for similar powder metallurgical approaches [2].

Some formation of aluminium carbide was observed but the reaction only appeared during the hot compaction step. After milling even up to 20 h, no Al_4C_3 could be detected even with high energy X-rays. In some cases, only the surface of the CNT is converted into aluminium carbide as observed by Perez-Bustamante et al. [15] and Ci et al. [16].

Conclusion

Aluminium alloy AlMg5 was reinforced with six different CNTs by planetary ball milling, powder degassing, and uniaxial hot compaction.

The nature of the CNT or their starting agglomeration states did not play a notable role in the mechanical performance of the fabricated composites. With all the investigated CNTs, outstanding mechanical strengths were achieved. The highest UTS values around 720 MPa were achieved with the lowest CNT content (0.5 vol%). This is exceeding 2 to 3 times the highest values reported for 5xxx series Al-alloys. The elaborated composites however are still brittle with elongation at rupture around 1 to 2 %.

The importance of milling time was investigated and it was concluded that uniaxial hot pressing is insufficient for compacting flake like powders resulting from short milling times. The longer milled blends with equiaxed morphologies were compacted successfully.

High energy ball milling leads to a decrease by a factor of 2 of the aluminium crystallite size. No strong clustering of the nanomaterials could be observed by electron microscopy.

This study demonstrated the effective ways to increase hardness and strength of materials via reinforcing it with different CNTs. The problem of limited ductility remained and this was addressed more thoroughly in next study.

3.2.2 Al_2O_3 reinforced MMCs

As carbon based reinforcement materials led to formation of hard but brittle aluminium carbide, also known for its poor corrosion resistance, aluminium oxide nanoparticles were proposed as reinforcement material to investigate how to tailor the composites ductility. Therefore AlMg5 alloy was mixed with 1 vol% Al_2O_3 (Alu65) nanoparticles using Retsch PM400 planetary ball-mill with standard milling procedures (described in section 2.2), varying the milling time and PCA.

Two surfactants, the stearic acid and heptane were used. The stearic acid ($CH_3(CH_2)_{16}CO_2H$) avoids the agglomeration of the particles due to the long molecular chain. Stearic acid has an affinity towards the surface of Alumina (Fig. 22) and due to its long C- chain is a very good potential candidate as surfactant for the alumina reinforcement nanoparticles. Heptane (C_7H_{16}) in other hand have less carbon content meaning introducing less carbon to the composite system. But as heptane has no particular affinity to aluminium or its oxide, then heptane is also less effective as PCA, meaning more heptane is needed to be effective.

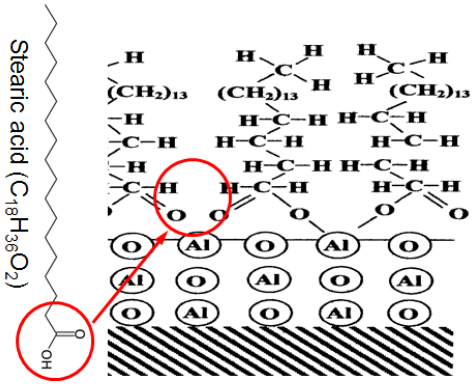

Figure 22. Schematic adsorption of SA on an alumina surface [4].

It was found out that using heptane as PCA led to equiaxed particles in shorter milling times than when using stearic acid. However, mechanical strength was superior when using SA compared to heptane (Fig. 23). The crystallite size was measured using XRD and is presented along other mechanical properties in Table 4. As can be seen in Table 4, heptane as PCA leads to smaller crystallite sizes and an increase of the mechanical strength of the AlMg5-1 vol% Alu65 composite already after the blend was milled for 6 hours. Nevertheless the hardness does not increase and the crystallite size is not decreased while prolonging the milling.

On the contrary, milling with SA as PCA induces a constant increase in hardness and decrease in crystallite size until 20 h of milling. Further increasing the milling time to 30 h leads indeed to an increase in hardness, but ductility was reduced compared to 20 h milling. Therefore optimised milling duration was considered to be 20 h.

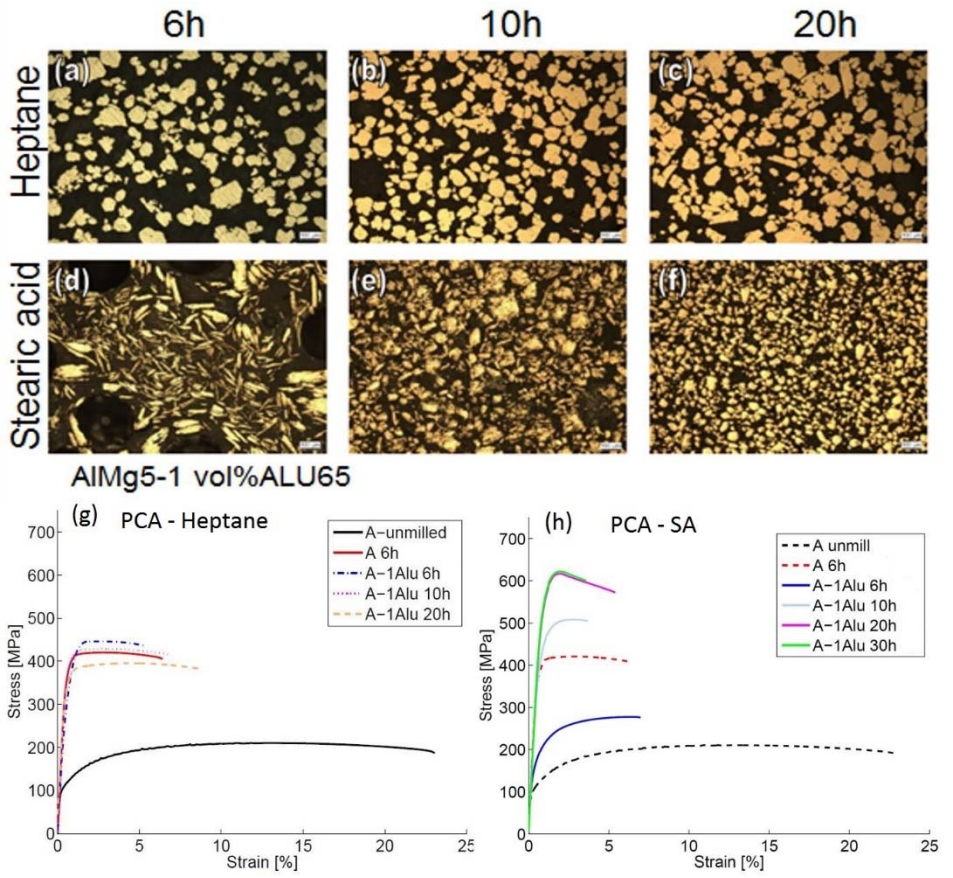

Figure 23. Influence of PCA and milling time on powder morphology and mechanical properties. a, b, c were milled with heptane while d, e, f were milled with stearic acid. g and h correspond to UTS of samples milled with heptane or stearic acid respectively.

Table 4. Mechanical properties and crystallite size of AlMg5-1 vol% Alu65 composites.

Composition	HV [HV20]	UTS [MPa]	Elongation [%]	Scherrer crystallite Size [nm]
AlMg5 unmilled	60	210	22	200
AlMg5 6h (hept)	120	420	5.5	100
1 vol%Alu65 6h SA	80	270	6	175
1 vol%Alu65 10h SA	140	510	2.8	120
1 vol%Alu65 20h SA	170	620	3.6	75
1 vol%Alu65 30h SA	180	600	1.9	80
1 vol%Alu65 6h hept	130	450	3.2	90
1 vol%Alu65 10h hept	130	420	4.7	90
1 vol%Alu65 20h hept	120	400	8	105

The mechanical properties of bulks compacted from powders with different morphology varied largely. As can be seen in Table 4, the 6h milled composite using stearic acid as PCA led to mechanical strength of only 270 MPa, while the same composite milled for 20 h led to UTS of 620 MPa. There was also a clear difference on powder morphology (Fig. 23), therefore the fracture surfaces of UTS samples were also investigated (Fig. 24). In Figure 24 and Table 4 one can see a connection between flake powder morphology, large crystallite size, fracture surface containing pulled-out flakes and low UTS value. And in the same time similar connection is clear between equiaxed powder morphology, reduced crystallite size, fracture surface with dimple fractures and high UTS value.

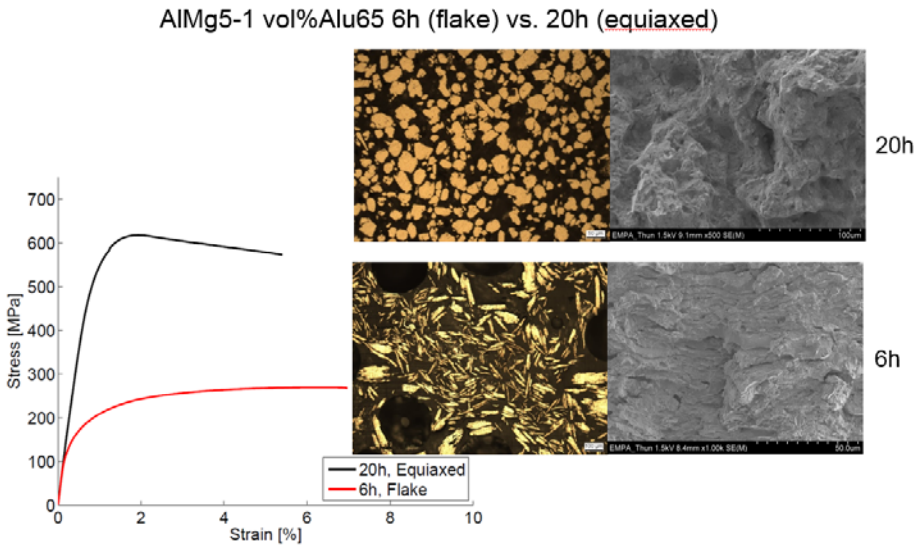

Figure 24. Powder cross sections, stress-strain curves and fracture surfaces of 6 h and 20 h milled AlMg5-1vol%Alu65 composite.

In order to gain information on the importance of content of PCA, a study was conducted with clear excess of stearic acid in AlMg5-1Alu65 composite. Blends were milled for 6 to 30 h with 1.5 wt%, 2.25 wt% and 3 wt% PCA. It was expected that such excess of stearic acid leads to a covering of the alumina particles with several layers of molecules, thus inhibiting powders ability to cold weld, leading to flake-like particles.

Estimations of the SA amount necessary for full coverage of the alumina nanoparticles was made based on an alumina adsorption area for each SA molecule of 0.3 x 0.3 nm [4] and on the BET particle specific area measurements. The calculations showed that the 1 vol% of 23 nm particles would require one third of the PCA respectively for reinforcement. This estimation is formulated by assuming a complete coverage of the reinforcement particles with a monolayer of SA, and is hence an upper boundary to the amount of PCA adsorbed on the reinforcement. As stearic acid does probably melt due to heating during ball-milling and hence be able to have contact with the whole alumina particles surface, it is important to take this phenomenon into account.

Heptane, does not have any functional group; it is only composed of a carbon and hydrogen backbone. This, combined with its relatively low molecular weight means that it will probably neither adsorb at the surface of alumina, nor at the fresh aluminium fracture surfaces. Therefore, it does not have a localized lubrication effect like SA, but will rather lead to a more statistical distribution. This explains why a 10-fold amount of heptane is used compared to SA. It does

probably not impede too much cold-welding between particles, but reduce the efficiency of ball impacts by introducing sliding between balls and particles. This could be the reason for a lower grain refinement and work-hardening compared to milling with SA. The crystallite sizes for all millings done with heptane and 23 nm particles (or even pure AlMg5 powder) are indeed very similar (49 nm for powder crystallites), and comparatively higher than in millings conducted with SA for 20h (35 nm).

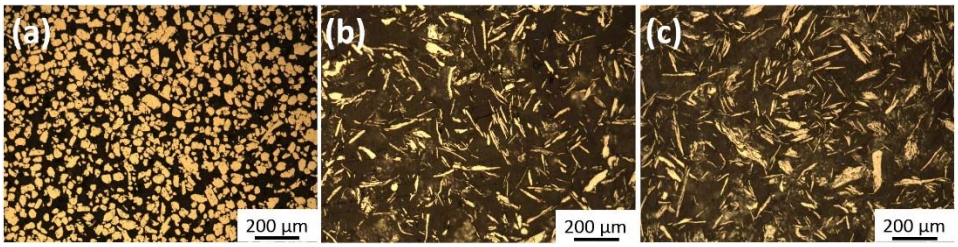

Figure 25. Powder morphology of 30 h milled AlMg5-1 vol% Alu65 blend with; A) 1.5 wt% stearic acid, B)2.25 wt% stearic acid, C) 3wt% stearic acid as PCA.

A TEM study of AlMg5-1 vol% Alu65, 20h bulk samples was carried out on samples cut from tensile specimens. Considering the low representativeness of TEM analyses, 6 samples were prepared and many images were taken. These characterizations revealed mainly homogenously distributed nanoparticles, but also some agglomerates of alumina nanoparticles and aluminium carbide (Al_4C_3) as shown in Figure 26.

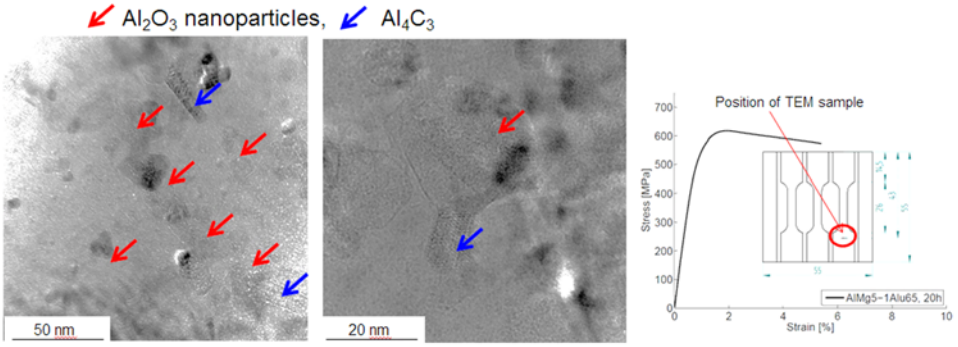

Figure 26. TEM analysis of AlMg5-1 vol%Alu65 composite made out of the 20 h milled blend, showing Al_2O_3 nanoparticles and some formation of Al_4C_3 phase.

Conclusions

To conclude the study on oxide based reinforcement, it could be stated that it is beneficial to use Al_2O_3 nanoparticles as reinforcement due to increased ductility with retained high strength. The powder metallurgy approach used was promising to produce aluminium matrix composites with attractive mechanical properties. The ductility was improved compared to composites reinforced with CNTs while the UTS remained high.

The importance of PCA for milling of AlMg5 with a low volume fraction of alumina reinforcement has been established. Milling the alloy with 1 vol% of reinforcement and 15 wt% heptane did not provide fine powder morphology for any of the milling times investigated in this report. The crystallite size did not reduce enough to contribute to strengthening, therefore these composites never reached a UTS higher than 450 MPa.

Milling AlMg5 with alumina nanoparticles and 1.5 wt% SA leads to different powder morphologies, from flakes to very fine equiaxed particles as the milling time increases. This behaviour, which depends on the amount of reinforcement particles, their size and the milling time, is attributed to the adsorption of SA on the alumina surface. Therefore, one has to tailor the level of SA addition for different particle sizes and volume fraction by calculating the amount necessary for full coverage of the alumina reinforcement particles with adequate surplus of PCA to hinder excessive cold welding. Furthermore, for a fixed amount of stearic acid (no additional SA introduced during milling), increase milling time progressively destroys and entraps SA in particles leading to shortage of PCA.

A link between powder morphology and tensile properties could thus be established, and it was found that the best suited morphology for composites compacted by hot pressing is a homogeneous blend composed of small and equiaxed particles. The previous conclusions on the role of stearic acid on milling can be used to obtain this morphology.

3.3 Milling and hot pressing. The cube milling

A new milling system, called cube mill, consisting of a square vessel moving in planetary movement was used to increase the milling energy and thereby shortening the milling time required for optimized powder morphology [37]. Optimization of milling parameters for cube mill was carried out based on the theory proposed by Fogagnolo et al. [6]. The milling was considered to be completed, after equiaxed powder morphology was achieved together with uniform particle size. After only three hours of milling with the cube mill, equiaxed powder morphology with uniform particle size was achieved. This is about six times faster than milling with a Retsch PM400 planetary ball mill that required up to 20 h for achieving similar milling state of the same composite

blend. For both milling systems, the mean particle size of the milled powder was about 40 μm (Fig. 27).

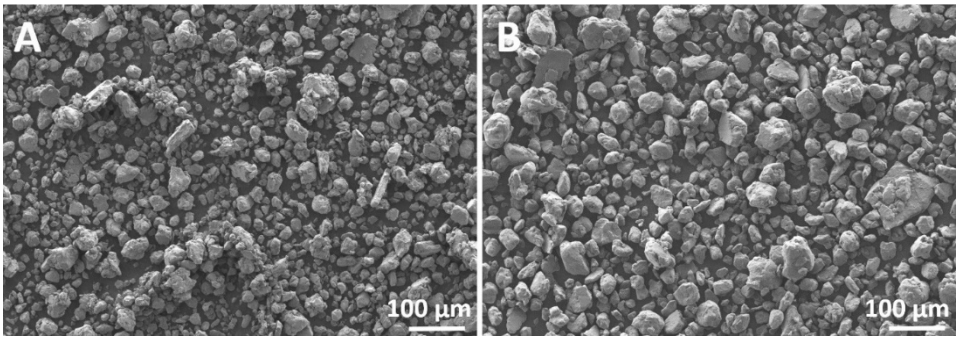

Figure 27. Examples of milled A-1.0np composite blends: A) blend milled with Retsch PM400 for 20 h [44]; B) blend milled with cube mill for 3 h [37]

After compaction, all the bulks possessed a density between 2.66 to 2.70 g/cm3, being close to the theoretical densities (2.64-2.66 g/cm3 depending on the reinforcement content). The amount of O_2 was measured before and after compacting and no significant oxidation was detected after high temperature compaction process (CHC) [Fig. 7,[37]].

The microstructure of compacted materials was characterised using EBSD, TKD and TEM to gain information about grain size, size distribution and orientation. The measured grain sizes and area fractions are presented in Table 5, while EBSD and TEM micrographs are shown in Fig. 28 and Fig. 30. The grains were measured in both axes relative to compacting direction, but no preferential orientation was observed. Unmilled AlMg5 (sample A_un) had an average grain size of 25 μm (Fig. 28A). No submicron grains were found; therefore it was considered that A_un had 100% coarse grain structure. The fraction of low angle grain boundaries recorded was relatively high for A_un (Fig. 29). After high energy milling, the fine grain structure appeared on A_m sample, exposing a bimodal grain structure consisting of both FG and CG areas (Fig. 28B). The amount of HAGB increased with a simultaneous decrease of LAGB, compared to A_un (Fig. 29). A similar microstructure was also seen for A-0.2np. Both A_m and A-0.2np had about 10% of FG area with grain size of 400 nm and remaining CG area with the grain size of 10 μm (see Table 5). After increasing the reinforcement content to 0.3 vol% (sample A-0.3np), the average size of coarse grains decreased to around 5 μm with concurrent increase of FG area to 50% (Fig. 3C). The grain size in the FG area decreased under the detection limits of conventional EBSD (dark unindexed area in Fig. 28C) therefore TEM was used to measure the average grain size of 300 nm for FG area. Further increase of the Al_2O_3 reinforcement induced a reduction of

the grains size and an increase of the FG area. Conventional EBSD was unable to sufficiently index grains with composites having reinforcement content 0.4 vol% (Fig. 28D) or higher, therefore TKD and TEM were used on these composites (Fig. 30). Average grain size in the CG area was reduced down to 1.4 µm for A-0.4np and 1.2 µm for A-0.5np (Fig. 30). No further grain refinement was recorded in CG area when increasing the nanoparticle content up to 1 vol% (A-1np, Fig.30). Both TEM and TKD gave a grain size around 250 nm for the fine grains (FG) for composites with reinforcement higher than 0.4 vol%. With the reinforcement volume fraction increasing, the amount of LAGB was reduced while the proportion of HAGB increased (Fig. 29) [37].

Table 5. Grain sizes and their surface fractions [37].

Composition	**Size of fine grains [µm]** d_{FG}	**Size of coarse grains [µm]** d_{CG}	**Area fraction of fine grains [%]** f_{FG}	**Calculated average grain size** $D = (f_{CG} \times d_{CG}) + (f_{FG} \times d_{FG})$ **[µm]**
A_un	-	25.00 ± 1.30	0	25.00
A_m	0.40 ± 0.02	10.00 ± 0.50	10	9.40
A-0.2np	0.40 ± 0.02	10.00 ± 0.50	10	9.40
A-0.3np	0.30 ± 0.02	5.00 ± 0.30	50	2.65
A-0.4np	0.25 ± 0.01	1.40 ± 0.07	70	0.60
A-0.5np	0.25 ± 0.01	1.20± 0.06	80	0.44
A-1.0np	0.25 ± 0.01	1.20± 0.06	90	0.34

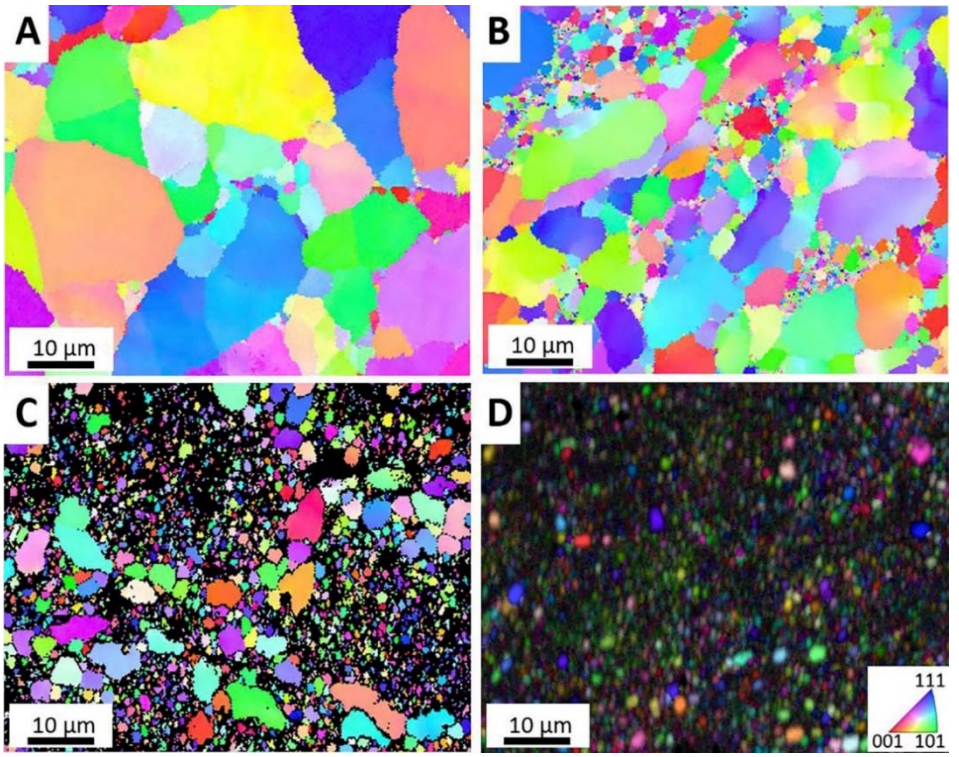

Figure 28. EBSD presenting GC regions: A) A_un consists only of CG; B) A_m showing bimodal grain structure with FG and CG regions; C) A-0.3np grain size have reduced and FG fraction (dark unindexed area) have increased with increasing reinforcement content; D) CG fraction have reduced significantly on A-0.4np with concurrent increase of FG content [37].

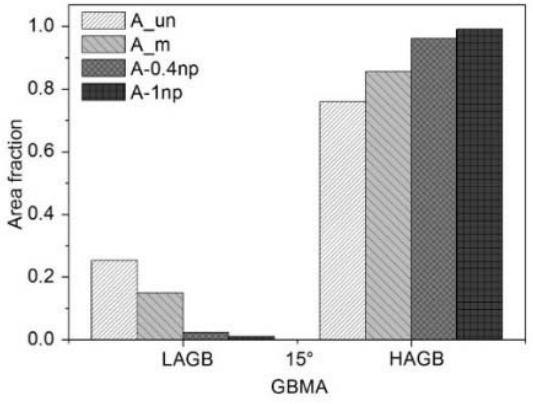

Figure 29. GBMA area fractions showing decrease of LAGB-s and increase of HAGB-s with milling and increasing reinforcement content [37].

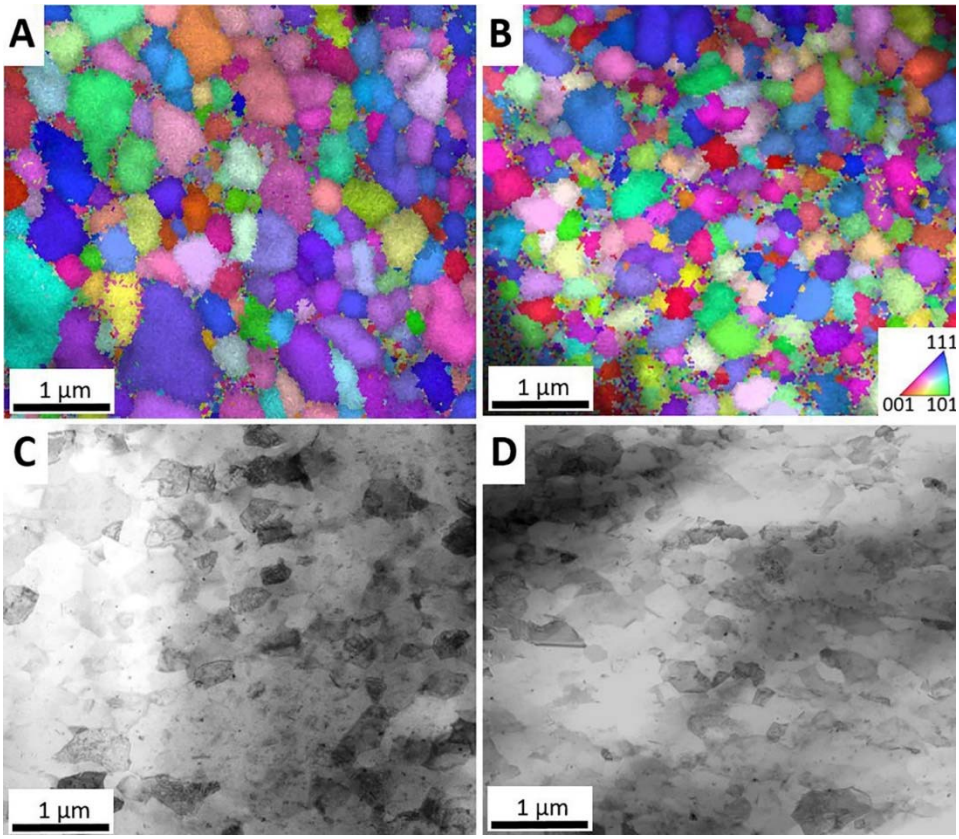

Figure 30. TKD maps with comparing TEM micrograph presenting FG regions of: A, C) A-0.4np; and B, D) A-1np composite [37].

To characterise the formation of Al_4C_3 on powder blends and the bulks, XRD was used. Al_4C_3 could be detrimental to the corrosion resistance and mechanical properties of the produced composites and is therefore unwanted. The Al_4C_3 phases could be observed only after the powder had undergone the CHC but not after high energy milling (Fig. 31). XRD data show a noticeable decrease of the crystallite size after milling from 90 to less than 40 nm. For all the composites the crystallite size after milling was indeed 30 to 40 nm. After hot compaction, the crystallite size increased about twofold whatever the composition of the material, reaching values around 90 - 100 nm. Finally, a shift of high angle peaks to higher 2Θ angles was observed, suggesting a release of residual strain during CHC (Fig. 31).

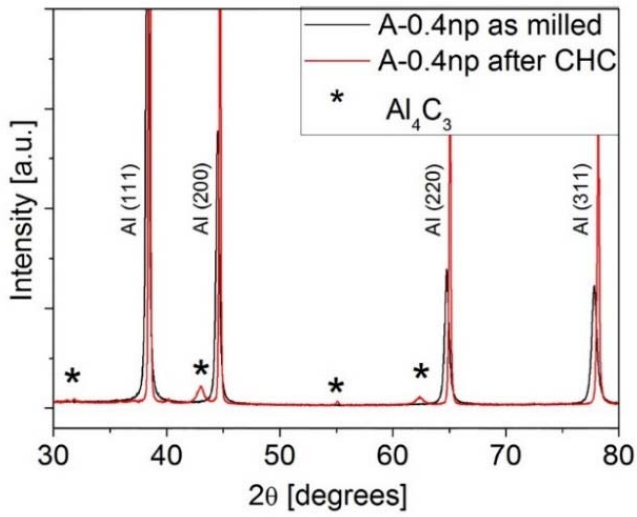

Figure 31. XRD of A-0.4np indicating crystallite growth (peak narrowing), formation of Al_4C_3 during CHC and release of residual strains (peaks are shifted after CHC) [37].

The highest mechanical strength of the investigated composites was achieved with the 1 vol% reinforcement content. Thus, Ultimate Tensile Strength (UTS) of 562 MPa, Yield Strength (YS) of 527 MPa and hardness of 160 HV20 were measured. However, this composite presented an elongation at rupture of 4 % (Fig. 32A) limiting their industrial applications. Reduced reinforcement contents led to lower tensile strength but to higher elongation at rupture (Table 6). Indeed already milling the unreinforced AlMg5 alloy (sample A_m) increased the hardness, UTS and YS as compared to unmilled AlMg5 (sample A_un) even if some minor decrease of elongation was noted. No additional strengthening was observed using only 0.2 vol% alumina nanoparticles over unreinforced A_m sample. Prominent increase of strength starts once reinforcement content increased to 0.3 vol% and above. Moreover, stress-strain curves show that UTS and YS values had become closer with increased reinforcement content, indicating to a poor additional strain hardening capability (Fig. 32A). A ductile fracture was confirmed by investigating fracture surfaces of UTS samples. A number of micro dimples and nucleated micro voids were found on the fracture surfaces of tested tensile specimens being an evidence of ductile fracture [45]. A typical fracture surface containing numerous dimples is presented for sample A-0.4np in Fig. 32B [37].

Table 6. Mechanical properties of compacted materials with standard commercial AA5083-H19 properties added for comparison [37].

Composition	UTS [MPa]	YS [MPa]	Elongation [%]	Hardness HV20
A_un (unmilled)	300±4	125±2	24.1±1.7	80±1
A_m (milled)	404±2	290±14	19.0±0.4	125±2
A-0.2np	399±2	285±6	19.2±0.5	119±1
A-0.3np	429±6	340±33	14.9±2.4	127±4
A-0.4np	466±7	426±26	11.0±1.9	141±3
A-0.5np	483±16	455±25	9.5±1	148±6
A-1.0np	562±6	527±21	4.0±1.3	158±6
AA5083-H19	*420*	*370*	*5*	*120*

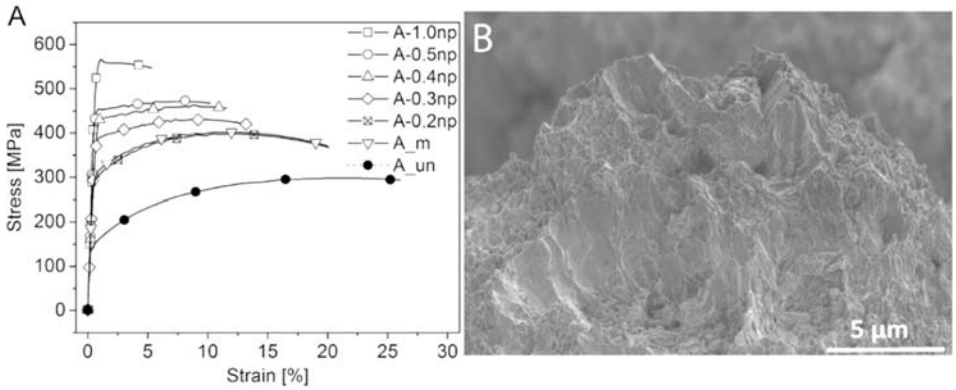

Figure 32. A) Stress-strain curves of cube milled and hot pressed bulks demonstrated an increase of UTS and YS with the reinforcement content increasing in conjunction with the reduction of ductility; B) dimples on the fracture surface indicating ductile fracture of A-0.4np [37].

High temperature testing

Obtained mechanical properties induced interest on high temperature capabilities of current material. Therefore annealing at 450 °C for 2 h under vacuum was conducted to compacted samples (Fig. 33). Interestingly after the samples had cooled down to room temperature, the mechanical properties were essentially the same as without annealing indicating a good high temperature stability.

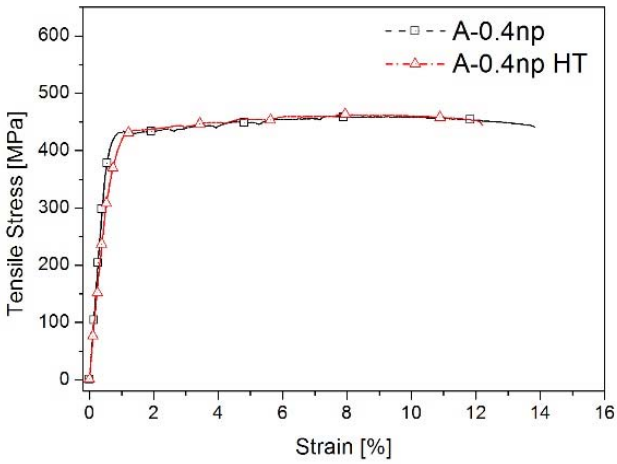

Figure 33. Tensile stress-strain curves of A-0.4np after compaction and after subsequent annealing at 450 °C for 2 h (A-0.4np-HT).

In order to verify the strength at high temperature, tensile tests were conducted at 200 °C (Table 7). It could be stated that the strength of material is reduced during high temperature, and even more dramatically for the reinforced composites. Interestingly tough the reinforced composite seems to have near superplastic properties, demonstrating elongation up to 44 % for A-0.5np composite.

Table 7. Tensile properties of samples tested at room temperature (RT) and at 200 °C [46].

Composition	**YS [MPa]**		**UTS [MPa]**		**Elongation [%]**	
	RT	200 °C	RT	200 °C	RT	200 °C
A_um	135±2	116±1	300±4	141±1	22±2	12±1
A_m	289±14	161±1	401±4	182±2	19±1	4±1
A-0.5np	455±25	73±2	483±16	108±5	10±1	44±5

RT – room temperature

The high temperature testing leads to interesting results indicating that the produced composites are having near superplastic and relatively soft state at elevated temperature (200 °C). But even after holding the composite at T_m0.8 (450 °C) for 2 h, once cooled down to room temperature, the previous mechanical properties are restored.

Discussion

Using a simple fabrication procedure leads to outstanding hardness and strength of aluminium nanocomposites. Indeed, twofold increase in hardness from 80 to 160 HV20 and fourfold increase in tensile yield strength from 125 to 530 MPa could be achieved with only 1 vol% of Al_2O_3 nanoparticles dispersed in the AlMg5 matrix (Table 6). The strength alone was not the whole story. The obtained combined strength and ductility was higher than reported for commercial 5xxx alloys (Fig. 34). Compared to CNT reinforced MMCs involved in current thesis, the strength achieved was slightly lower, but fivefold increase in elongation was achieved, making the material industrially usable. Higher strength has been achieved also before by other authors, but all of these researchers have used secondary processing steps such as HIP, forging or extrusion after initial compaction to overcome the native oxide layer on particle surfaces and induce ductility [2, 47–49]. In current work a technique was proposed which allows to obtain similar mechanical properties for near net shaped objects with only one step compaction process [37].

Achieved outstanding mechanical properties together with microscopy analyses indicated that cube milling is a more efficient high energy ball-milling process than planetary ball-milling with cylindrical vessels. The cube shaped vessels seemed to have advantages over cylindrical walled milling vessels. Authors proposed that the main advantages are coming from impact forces when milling balls are hitting flat wall over shearing forces presented by round shaped vessels during ball milling.

Knowing that applying heat to cold worked metal leads to recrystallization and grain growth [50], which in term is linked to a decrease of the strength, as described by the Hall-Petch mechanism, a sufficient time and temperature is still required for degassing and successful compacting the milled aluminium composite blend [39]. Compromise parameters for temperature and time of the compaction heating cycle were therefore chosen. A twofold growth in crystallite size and some strain release from cold worked blend, which was also reported by Wagih et al. [51], was detected with XRD after compacting the composite blend (Fig. 6 in [37]). Additionally, elevated temperature of CHC led to the formation of Al_4C_3 (Fig. 9A in [37]) that could be disadvantageous due to possible occurrence of galvanic corrosion between carbon and Al materials in the composite [52].

The microstructure was thoroughly investigated and the uniaxially hot pressed samples having an isotropic grain structure was confirmed. The unmilled AlMg5 alloy (A_un) possessed mainly coarse grained microstructure with an average grain size of 25 µm (Fig. 28A and Table 5) and a large amount of low angle grain boundaries compared to the other materials (Fig. 29). Hot pressing in a uniaxial press was not providing sufficient cold work i.e. severe plastic deformation, so the assumption could be made that the compacts were in annealed state. Three hours

of high energy milling without reinforcement reduced the size of coarse grains and introduced regions of fine grains, leading to a bimodal grain microstructure. The amount of LAGBs was reduced and inversely HAGBs increased. Adding 0.2 vol% reinforcement to the matrix induced neither significant changes in the microstructure nor in the mechanical properties compared to A_m. From 0.3 vol% onwards, the amount of fine grains increased drastically with the decrease of grain size in both FG and CG regions. Also, the amount of HAGBs increased due to strain hardening. Even though the grain size further decreased with the reinforcement content increasing up to 1 vol%, the main structure remained bimodal with a certain amount of micron sized coarse grains and submicron sized fine grains (Fig. 30). The mechanical strength increased with the reinforcement content while the ductility and the fraction of LAGBs decreased. This being in agreement with the literature stating that LAGBs are unfavourable for blocking dislocation movement over grain boundary, therefore providing ductility [27, 28]. In this study the exact effect of grain boundary orientation regarding plasticity was difficult to distinguish, as simultaneously volume fraction of nanoparticles is changed.

Under TEM investigations of the composites, several aluminium carbide structures were observed (Fig. 33A). XRD analyses confirmed these observations and indicated Al_4C_3 formation during the CHC process not during milling (Fig. 6 in [37]). TEM also revealed several rows of γ-Al_2O_3 nanoparticles that seem to have formed from the native oxide layer being present on the surface of milled particles (Fig. 33A and 33B). Balog et al. have described similar oxide nanoparticles at compacted particle boundaries for unmilled aluminium particles processed by hot pressing. The authors have described how the native amorphous oxide layer transformed into γ-Al_2O_3 at temperatures above 450 °C [42, 53]. Similar to Balog et al., author of this study supposes that these rows of γ-Al_2O_3 nanoparticles result from the breaking of the native oxide layer covering the particles during milling, followed by recrystallization during the high temperature cycle (Fig. 33C). Whereas Balog et al. were using monograin particles to simplify understanding of this process, in our case, the milled powder particles included several hundred grains and therefore the crystallized particles are not surrounding every single grain.

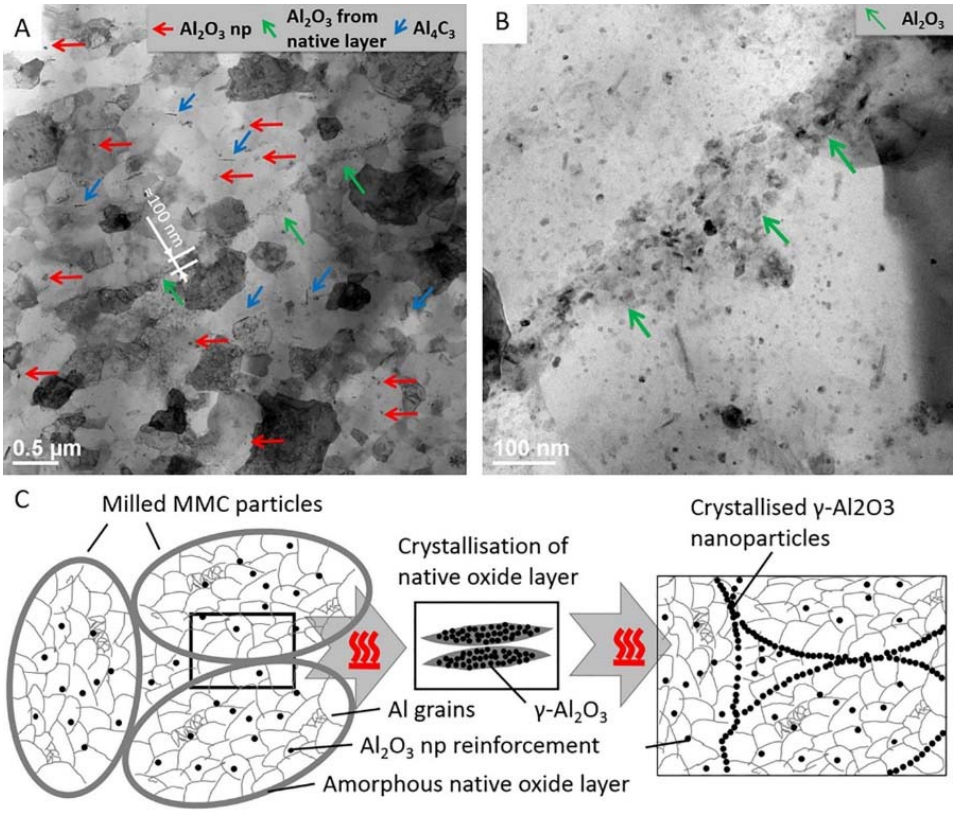

Figure 33. A) A-0.4np shows random distribution of nano-reinforcement. Al_4C_3 emerged from the reaction between stearic acid and aluminium. Native oxide layer crystallized to γ-Al_2O_3 nanoparticles. B) γ-Al_2O_3 nanoparticles formed from native oxide layer; C) proposed scheme for formation of nanoparticles from native oxide layer [37].

The fabricated composites possessed superior strength and ductility over any 5xxx and 6xxx series alloys. The UTS of some commercial alloys of named series are presented together with results from the study in Figure 34.

It can be noted that with increased reinforcement content, the UTS increases almost linearly while ductility decreases (Fig. 34). This means that the mechanical properties could then be tailored by adapting the reinforcement content. The mechanical properties were directly correlated with the changes in the microstructure which was correlated to the reinforcement content added to matrix. With the increase in reinforcement content, the decrease in mean grain size and the increase of the fraction of FG regions, the strength of the material increased with simultaneous reduction of ductility. Even though the ductility was decreased, then compared to previous studies using similar material processing, the materials

that were achieved possessed considerably better ductility [2]. It is believed that the ductility is retained by CG regions in the bimodal structure [24] and the presence of LAGBs [28].

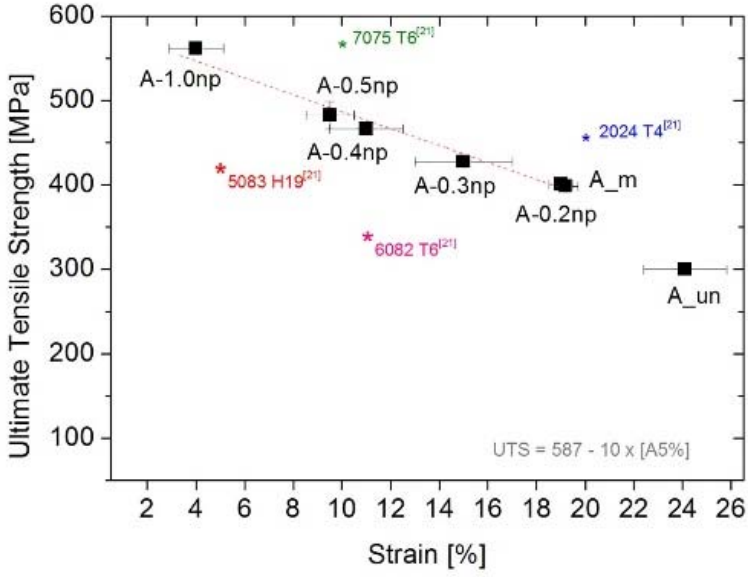

Figure 34. Ultimate tensile strength is evolving linearly with the reinforcement content increasing. Mechanical properties achieved are exceeding any 5xxx series commercial alloy (presented 5083-H19 as one of the strongest 5xxx alloys commercially available) [37, 54].

3.4 The strengthening mechanisms

Solid solution strengthening, grain boundary strengthening, Orowan strengthening and dislocation strengthening were considered to be the major mechanisms that contribute to the improvement of the mechanical properties of investigated MMCs.

Solid solution strengthening in AlMg5 alloy matrix results from an interaction between the mobile dislocations and the solute atoms. Based on the work of Ryen et al. [18], the constant values for equation 1 (section 1.1.4) were selected as follows: $\sigma_{pure} = 19.5$; H=12.1; C=5; n=1.14. This led to a solid solution strengthening in the AlMg5 matrix MMCs of 95 MPa.

The Orowan strengthening was calculated with the assumption that the second phase particles were equiaxed, non-shearable and small enough (< 1 μm). And for this calculation, the particle size distribution of the reinforcement was considered narrow and homogeneously distributed in the matrix. Values of σ_{OR} are reported in Table 7 for the different nanoparticle contents.

The native oxide layer that existed already before milling was also considered to be contributing to the Orowan strengthening, therefore, the calculated strengthening effect of 32 MPa was added to milled materials [37].

The grain-boundary strengthening is described by the Hall-Petch equation (Eq. (7), section 1.1.4) [21,22,55]:

As the composites present both coarse and fine grains, to calculate the strengthening mechanism, an average grain size was introduced based on a rule of mixture:

$$D = (f_{CG} \times d_{CG}) + (f_{FG} \times d_{FG}), \qquad (8)$$

where d_{CG} and d_{FG} represent the average grain size of coarse-grain and fine-grain regions, respectively and f_{CG} and f_{FG} represent the area fraction of coarse-grain and fine-grain regions, respectively. The average grain sizes are reported in Table 5, while the strengthening contributions of σ_{HP} are presented in Table 7.

Dislocation strengthening (σ_ρ) was calculated using the Taylor formula (Eq. (6), section 1.1.4) [20, 56] and is included in Table 8.

Table 8. The main strengthening mechanisms involved in this study [37]

Composition	Calculated σ [MPa]						Measured σ [MPa]
	σ_{SS}	σ_{ODS}	σ_{ρ}	σ_{OR}	σ_{HP}	$\sum\sigma$	σ_{Y}
A_un	95	0	0	0	44	120	125
A_m	95	32	16	0	60	188	290
A-0.2np	95	32	16	54	60	238	285
A-0.3np	95	32	20	68	93	289	340
A-0.4np	95	32	20	79	175	382	426
A-0.5np	95	32	20	89	201	418	455
A-1.0np	95	32	20	130	224	482	527

σ_{SS}- Solid solution strengthening; σ_{ODS}- Orowan strengthening from ODS effect of native oxide layer; σ_{ρ} – dislocation strengthening; σ_{OR} - Orowan strengthening from reinforcement; σ_{HP} - Hall-Petch strengthening; $\sum\sigma$: Sum of calculated strengthening effects; σ_{Y}: 0.2 % measured offset yield strength.

The theoretical strength values were in agreement with the measured mechanical properties, even if always lower. The discrepancy is more pronounced for the unreinforced sample. The addition and dispersion of nanoparticulate material in the matrix increases the contribution of grain refinement and Orowan strengthening significantly. These became then the major mechanisms for improving the strength of the composite. The ODS mechanism as well as the dislocation strengthening have only minor contribution regarding the high yield strengths achieved for the investigated nanocomposites.

These calculations indicated clearly that milling is an important processing step to achieve superior mechanical properties in metal matrix composites reinforced with nanoparticles. Beside the dispersion function (Orowan), milling also decreases the grain size of the matrix. The milling efficiency is also improved by the addition of nanoparticulate materials over a minimal amount (in this study > 0.2 vol%).

Conclusion

A simple one-step process was used in this study. The process that consisted of cube milling and uniaxial hot pressing, enabled achieving high strength and ductile net shape products without the need for secondary operations. Cube milling was six times faster than commercially available planetary ball mill for obtaining homogeneous blend. Mechanical properties of the composites exceeded commercial 5xxx alloys simultaneously in strength and ductility. UTS of up to 562 MPa with YS of 527 MPa and elongation at rupture of 4% was achieved with 1 vol% of nano-Al_2O_3 reinforcement. The strength-ductility combination of the composites was tailored by adjusting the nanoparticulate material content between

0.3 and 1 vol%. Solid solution strengthening, Orowan strengthening and grain boundary strengthening were found to be the main mechanisms contributing to strengthening and achieving high strength while the bimodal grain structure in collaboration with LAGBs were believed to be the main source of retained ductility.

3.5 Study of alternative compaction methods

During the thesis several compaction methods were evaluated in order to find the best compaction technique. For simpler comparison, all the alternative processing routes used the same processing temperature of 550 °C. In following main results are discussed shortly to give oversight of the influence of different compaction methods to Al-MMCs.

Spark Plasma Sintering

Cube milled Al-MMC powders were successfully compacted to full density with Spark Plasma Sintering technology [30]. Being fast and efficient compacting method SPS produced sintered samples in short time. Unfortunately the SPS method is still not broadly accepted industrial method but still used mostly in laboratories.

The compacted Al-MMCs possessed somewhat lower strength values, compared to hot pressed samples. The YS of AlMg5-0.4 vol% Al_2O_3 was noticeably lower than YS achieved by hot pressing (Fig. 35A) whereas the difference in UTS was not important. It seems that samples compacted with SPS were in less work hardened state than samples compacted with hot pressing.

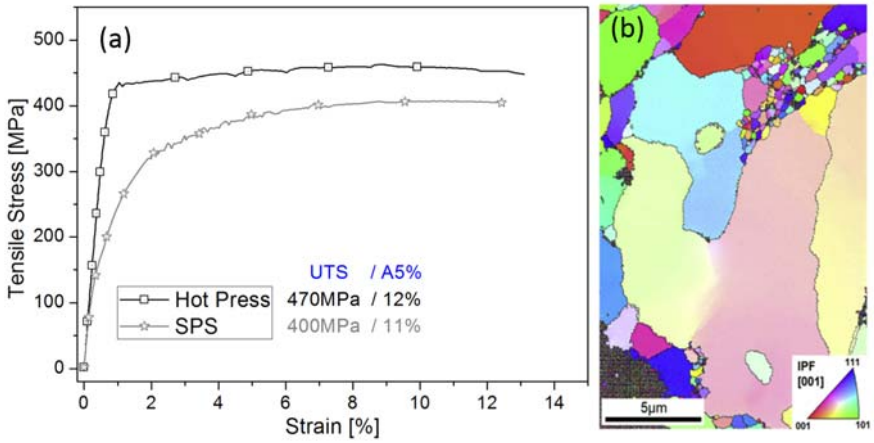

Figure 35. A) Tensile stress-strain curves of SPS compacted cube milled Al-MMC composite blends. AlMg5-UM – unmilled alloy, AlMg5-M – cube milled, but unreinforced alloy. B) Transmission EBSD of the spark plasma sintered sample AlMg5–0.4Al_2O_3, black lines: high angle grain boundaries [30].

This is also corroborated by the microstructure (Fig. 35B). The 0.4 vol% reinforced sample compacted by SPS possessed bimodal grain structure, similar to HP sample. The difference however was the larger average size of coarse grains around 8 ± 2 μm (in the case of HP 1.2 μm). Fine grains were about the same size averaging around 250 to 300 nm. Considering that the compactions were made out of the same powder the difference in microstructure is noticeable and it is clear that more grain growth and recovery has been taking place during the short time used in SPS. It is very interesting to see higher level of grain growth during 15 min of SPS heating, compared to several hours of conventional heating and further research is planned to clarify this question.

Spark plasma sintering can achieve fully dense bulk Al-MMCs out of high energy milled composite blends. It seems that the grain growth is more prominent tough in the case of SPS, compared to traditional hot pressing. This in terms leads to lower UTS and YS values to achieve with SPS technology.

Hot Isostatic Pressing

Hot Isostatic Pressing was conducted on AlMg5–0.4Al_2O_3 powder blends to investigate the effect of isostatic pressure. The blends were capsulated, sealed and HIP-ed. Compared to uniaxial hot pressing the HIP did not lead to noticeable increase in ductility. The UTS and YS were smaller compared to hot pressed samples (Fig. 36).

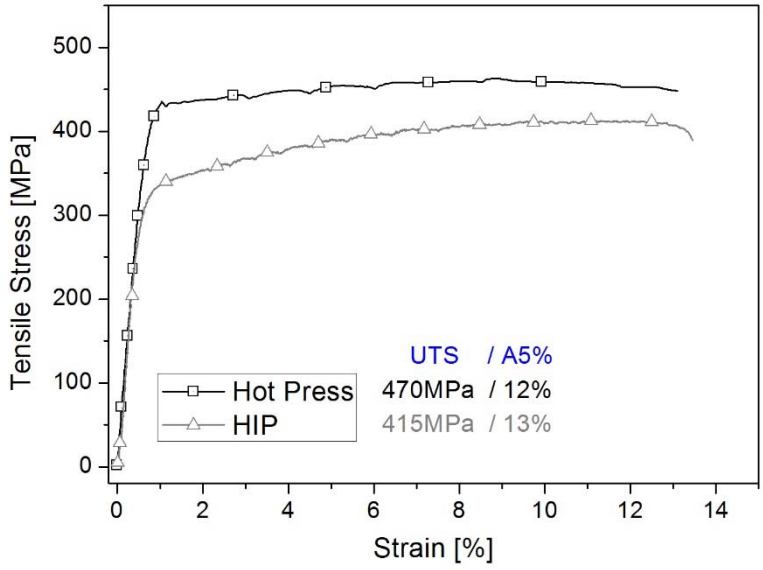

Figure 36. Stress-strain curves of HIP-ed and hot pressed AlMg5–0.4Al_2O_3 samples.

The bimodal grain structure consisted of slightly larger grains that in the case of HP samples. The grain sizes were more similar to SPS samples than to HP samples (Fig. 37).

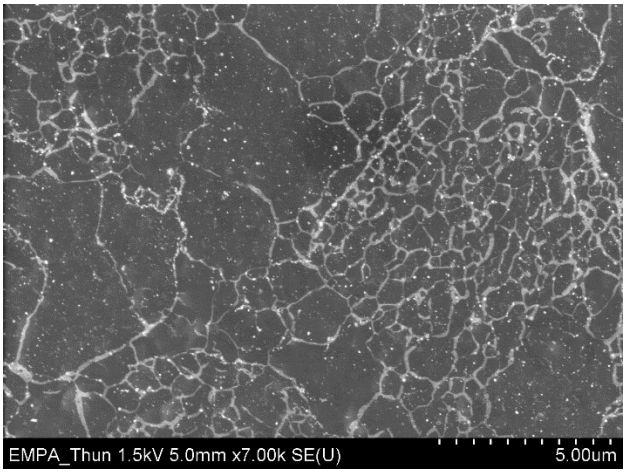

Figure 37. A bimodal grain structure of AlMg5–0.4 vol% Al_2O_3 revealed under SEM after Ar-ion polishing.

Hot forging

Hot forging was investigated as a mean to promote metal-metal contact through plastic deformation. Slight improvement of ductility was observed in all the samples compared to other compacting methods. Nevertheless also a decrease in YS was observed compared to hot pressing (Fig. 38). The microstructural studies were not finalized and therefore it is impossible to say at the time of writing the thesis whether the decrease in YS was caused by recovery and grain growth.

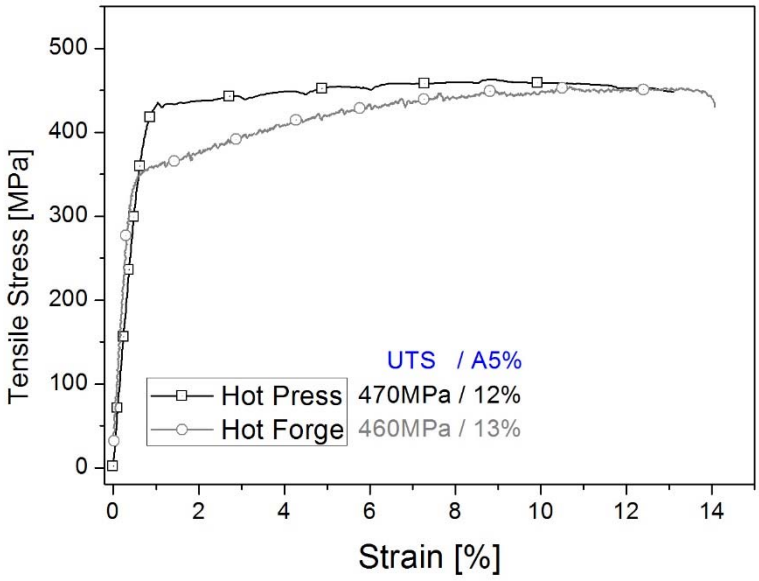

Figure 38. Stress-strain curves of hot pressed and hot forged AlMg5–0.4Al_2O_3 samples.

Conclusion

Some widespread alternative compaction methods were investigated but it seemed that in all the cases the YS was lower than in the case of hot pressed samples. Additionally no significant improvement in ductility over HP was observed. Bimodal grain structure was present, but consisted of somewhat larger grains than in the case of HP. The lower YS and larger grain size indicate lower state of work hardening and more pronounced grain growth in the case of alternative compacting routes. Therefore it can be stated that hot pressing was very well optimized for compacting of Al-MMC blends and no significant improvement could be achieved with alternative compacting methods.

4. CONCLUSIONS

High energy milling is an efficient method to disperse nanoparticulate materials in ductile matrix, to achieve MMCs with improved mechanical properties. Uniaxial hot pressing, method developed in this work, is a simple but efficient approach for processing aluminium based composites. With optimised set of parameters high density and outstanding mechanical performance can be achieved, and therefore the formulated goals in section 1.2 could be achieved:

- The main processing parameters are ball milling for homogeneous dispersion and heating temperature to allow sufficient plastic yielding during hot pressing, which have to be taken into account in order to create high strength ductile MMC using minimal processing steps.
    - High strength (UTS 470 MPa) combined with outstanding ductility (>11 %) was achieved by dispersing 0.4 vol% Al_2O_3 nanoparticles in AlMg5 matrix. The concurrent strength and ductility was achieved with cube milling and uniaxial hot pressing without any additional processing steps.
- The microstructure of the high strength – high ductility MMCs needs to contain coarse grains dispersed between ultrafine or nanograins in order to blunt evolving cracks during deformation. Related features and impact of these on mechanical properties of MMCs are as follows.
    - By adjusting the nanoparticulate material content in MMCs, the microstructure of MMC can be tailored.
        - The increase in reinforcement content leads to increase of fine grained structure and HAGBs in microstructure that are contributing to high strength of MMC.
        - Coarse grains in conjunction with LAGBs are contributing to retained ductility of MMC.
        - Bimodal microstructure consisting both CG and FG regions combined with concurrent HAGBs and LAGBs provide exceptional strength-ductility combination of the composite.

- The strengthening mechanisms involved were evaluated
    - Grain boundary strengthening and Orowan strengthening were the two dominant strengthening mechanisms. Indicating that both MM and addition of second phase particulates play important role in achieving high strength MMCs.
- Near-superplastic properties with exceptional temperature stability of created MMC were observed.
    - At 200 °C the composite had near superplastic properties. Once cooled down no degradation of mechanical properties was observed.
    - Annealing the MMC for 2 h at 450 °C left no degradation of mechanical properties once cooled down indicating in exceptional temperature stability.

The novelty of presented research can be outlined by.

- Developed and implemented new high energy milling system with angled square milling vessels.
- Developed method to produce near net shaped Al-MMCs with simultaneous strength and ductility without post processing.
- Presented methodology for tailoring the strength and ductility by modifying the reinforcement content and therefore microstructure of composite.

REFERENCES

[1] Miracle, D. B., “Metal matrix composites – From science to technological significance,” Compos. Sci. Technol., 2005, vol. 65, no. 15–16, pp. 2526–2540.

[2] Suryanarayana, C., and Al-Aqeeli, N., “Mechanically alloyed nanocomposites,” Prog. Mater. Sci., 2013, vol. 58, no. 4, pp. 383–502.

[3] Suryanarayana, C., “Mechanical alloying and milling,” Prog. Mater. Sci., 2001, vol. 46, no. 1–2, pp. 1–184.

[4] Shaw, L., Villegas, J., Luo, H., Zawrah, M., Miracle, D., “Effects of process-control agents on mechanical alloying of nanostructured aluminum alloys,” Metall. Mater. Trans. A, 2003, vol. 34, no. 1, pp. 159–170.

[5] Arias, A., “Chemical reactions of metal powders with organic and inorganic liquids during ball milling,” Nasa Technical Reports, NASA-TN-D-8015, 1975.

[6] Fogagnolo, J. B., Velasco, F., Robert, M. H., Torralba, J. M., “Effect of mechanical alloying on the morphology, microstructure and properties of aluminium matrix composite powders,” Mater. Sci. Eng. A, 2003, vol. 342, no. 1–2, pp. 131–143.

[7] Kollo, L., Leparoux, M., Bradbury, C. R., Jäggi, C., Carreño-Morelli, E., Rodríguez-Arbaizar, M., “Investigation of planetary milling for nano-silicon carbide reinforced aluminium metal matrix composites,” J. Alloys Compd., 2010, vol. 489, no. 2, pp. 394–400.

[8] Llorca, J., Poza, P., “Influence of matrix strength on reinforcement fracture and ductility in Al-Al2O3 composites,” Mater. Sci. Eng. A, 1994, vol. 185, no. 1–2, pp. 25–37.

[9] Kang, Y.C., Chan, S. L.-I., “Tensile properties of nanometric Al2O3 particulate-reinforced aluminum matrix composites,” Mater. Chem. Phys., 2004, vol. 85, no. 2–3, pp. 438–443.

[10] Samal, P.K., Newkirk, J.W., Ed., ASM Handbook, Volume 7: Powder Metallurgy. 1998.

[11] Deng,C., Zhang,X., Wang,D., Lin,Q., Li,A., “Preparation and characterization of carbon nanotubes/aluminum matrix composites,” Mater. Lett., 2007, vol. 61, no. 8–9, pp. 1725–1728.

[12] Bradbury,C.R., Gomon, J.K., Kollo, L., Kwon, H., Leparoux, M., "Hardness of Multi Wall Carbon Nanotubes reinforced aluminium matrix composites," J. Alloys Compd., 2014, vol. 585, pp. 362–367.

[13] Liu, Z. Y., Xu, S. J., Xiao, B. L., Xue, P.,. Wang, W. G., Ma, Z. Y., "Effect of ball-milling time on mechanical properties of carbon nanotubes reinforced aluminum matrix composites," Compos. Part Appl. Sci. Manuf., 2012, vol. 43, no. 12, pp. 2161–2168.

[14] Esawi, A. M. K., Morsi, K., Sayed, A., Taher, M., Lanka, S., "The influence of carbon nanotube (CNT) morphology and diameter on the processing and properties of CNT-reinforced aluminium composites," Compos. Part Appl. Sci. Manuf., 2011, vol. 42, no. 3, pp. 234–243.

[15] Pérez-Bustamante,R., Pérez-Bustamante, F., Estrada-Guel, I., Licea-Jiménez, L., Miki-Yoshida, M., Martínez-Sánchez, R., "Effect of milling time and CNT concentration on hardness of CNT/Al2024 composites produced by mechanical alloying," Mater. Charact., 2013, vol. 75, pp. 13–19.

[16] Ci, L., Ryu, Z., Jin-Phillipp, N.Y., Rühle, M.,"Investigation of the interfacial reaction between multi-walled carbon nanotubes and aluminum," Acta Mater., 2006, vol. 54, no. 20, pp. 5367–5375.

[17] Kwon, H., Takamichi, M., Kawasaki, A., Leparoux, M., "Investigation of the interfacial phases formed between carbon nanotubes and aluminum in a bulk material," Mater. Chem. Phys., 2013, vol. 138, no. 2–3, pp. 787–793.

[18] Ryen, Ø., Holmedal, B., Nijs, O., Nes, E., Sjölander, E., Ekström, H.E., "Strengthening mechanisms in solid solution aluminum alloys," Metall. Mater. Trans. A, 2006, vol. 37, no. 6, pp. 1999–2006.

[19] Orowan, E., "Die mechanischen Festigkeitseigenschaften und die Realstruktur der Kristalle," Z. Für Krist. - Cryst. Mater., 1934, vol. 89, no. 1, pp. 327–343.

[20] Ashby, M. F., "The deformation of plastically non-homogeneous materials," Philos. Mag., 1970, vol. 21, no. 170, pp. 399–424.

[21] Hall, E. O., "The Deformation and Ageing of Mild Steel: III Discussion of Results," Proc. Phys. Soc., 1951, Sect. B, vol. 64, no. 9, p. 747.

[22] Petch, N.J.J., "The Cleavage Strength of Polycristals," J Iron Steel Inst Lond, 1953, p. 25.

[23] Whang, S.H., "Nanostructured Metals and Alloys: Processing, Microstructure, Mechanical Properties and Applications." Elsevier, 2011.

[24] Tellkamp, V. L., Lavernia, E. J., Melmed, A., "Mechanical behavior and microstructure of a thermally stable bulk nanostructured Al alloy," Metall. Mater. Trans. A, 2001, vol. 32, no. 9, pp. 2335–2343.

[25] Ma, E., "Eight routes to improve the tensile ductility of bulk nanostructured metals and alloys," JOM, 2006, vol. 58, no. 4, pp. 49–53.

[26] Zhao, Y., Zhu, Y., Lavernia, E. J., "Strategies for Improving Tensile Ductility of Bulk Nanostructured Materials," Adv. Eng. Mater., 2010, vol. 12, no. 8, pp. 769–778.

[27] Canadinc, D., Biyikli, E., Niendorf, T., Maier, H. J. "Experimental and numerical investigation of the role of grain boundary misorientation angle on the dislocation–grain boundary interactions", Advanced Engineering Materials, 2011, 13(4), 281-287.

[28] Hu, T., Ma, K., Topping, T.D., Saller, B., Yousefiani, A., Schoenung, J.M. and Lavernia, E.J., "Improving the tensile ductility and uniform elongation of high-strength ultrafine-grained Al alloys by lowering the grain boundary misorientation angle." Scripta Materialia, 2014, 78, pp.25-28.

[29] Dieter G.E., Mechanical Metallurgy. New York: McGraw-Hill Book Co., 1988.

[30] Babu, N. K., Kallip, K., Leparoux, M., AlOgab, K.A., Maeder, X., Arroyo-Dasilva, Y., "Influence of microstructure and strengthening mechanism of AlMg5–Al2O3 nanocomposites prepared via spark plasma sintering," Mater. Des., 2016, vol. 95, pp. 534–544.

[31] Kallip, K., Leparoux, M., AlOgab, K.A., Clerc, S., Deguilhem, G., Arroyo, Y. and Kwon, H., "Investigation of different carbon nanotube reinforcements for fabricating bulk AlMg5 matrix nanocomposites", Journal of Alloys and Compounds, 2015, 646, pp.710-718.

[32] Tessonnier, J.P., Rosenthal, D., Hansen, T.W., Hess, C., Schuster, M.E., Blume, R., Girgsdies, F., Pfänder, N., Timpe, O., Su, D.S. and Schlögl, R., "Analysis of the structure and chemical properties of some commercial carbon nanostructures", Carbon, 2009, 47(7), pp.1779-1798.

[33] Smajda, R., Mionic, M., Duchamp, M., Andresen, J. C., Forró, L., Magrez, A., "Production of high quality carbon nanotubes for less than $1 per gram," Phys. Status Solidi C, 2010, vol. 7, no. 3–4, pp. 1236–1240.

[34] Magrez, A., Seo, J.W., Smajda, R., Korbely, B., Andresen, J.C., Mionic, M., Casimirius, S., Forró, L "Low-Temperature, Highly Efficient Growth of Carbon Nanotubes on Functional Materials by an Oxidative

Dehydrogenation Reaction," ACS Nano, 2010, vol. 4, no. 7, pp. 3702–3708.

[35] Delmas, M., Pinault, M., Patel, S., Porterat, D., Reynaud, C., Mayne-L'Hermite, M., "Growth of long and aligned multi-walled carbon nanotubes on carbon and metal substrates," Nanotechnology, 2012, vol. 23, no. 10, p. 105604.

[36] Pinault, M., Mayne-L'Hermite, M., Reynaud, C., Beyssac, O., Rouzaud, J. N., Clinard, C., "Carbon nanotubes produced by aerosol pyrolysis: growth mechanisms and post-annealing effects," Diam. Relat. Mater., 2004, vol. 13, no. 4–8, pp. 1266–1269.

[37] Kallip, K., Babu, N.K., AlOgab, K.A., Kollo, L., Maeder,X., Arroyo, Y., Leparoux, M., "Microstructure and mechanical properties of near net shaped aluminium/alumina nanocomposites fabricated by powder metallurgy". Journal of Alloys and Compounds, 2017, 714, pp.133-143.

[38] Kallip, K., Kollo, L., Leparoux, M., Bradbury, C. M., "Nanoparticulate Reinforced Aluminum Alloy Composites Produced by Powder Metallurgy Route," Advanced Composites for Aerospace, Marine, and Land Applications II, 2015, pp. 165–174.

[39] Zhang, Z., Topping, T., Li, Y., Vogt, R., Zhou, Y., Haines, C., Paras, J., Kapoor, D., Schoenung, J.M., Lavernia, E.J., "Mechanical behavior of ultrafine-grained Al composites reinforced with B4C nanoparticles", Scripta Materialia, 2011, 65(8), pp.652-655.

[40] Choi, H. J., Shin, J. H., Bae, D. H., "The effect of milling conditions on microstructures and mechanical properties of Al/MWCNT composites," Compos. Part Appl. Sci. Manuf., 2012, vol. 43, no. 7, pp. 1061–1072.

[41] Zhang, Z., Topping, T., Li, Y., Vogt, R., Zhou, Y., Haines, C., Paras, J., Kapoor, D., Schoenung, J.M., Lavernia, E.J., "Mechanical behavior of ultrafine-grained Al composites reinforced with B4C nanoparticles," Scr. Mater., 2011, vol. 65, no. 8, pp. 652–655.

[42] Balog, M., Poletti, C., Simancik, F., Walcher, M., Rajner, W., "The effect of native Al2O3 skin disruption on properties of fine Al powder compacts," J. Alloys Compd., 2011, vol. 509, Supplement 1, pp. S235–S238.

[43] Esawi, A. M. K., Morsi, K. Sayed, A. Taher, M., Lanka, S., "Effect of carbon nanotube (CNT) content on the mechanical properties of CNT-reinforced aluminium composites," Compos. Sci. Technol., 2010, vol. 70, no. 16, pp. 2237–2241.

[44] Clerc, S., “Improvement of Aluminum Composites With Nanoparticulate Materials,” EPFL, Switzerland, 2014.

[45] Anderson, T. L. “Fracture Mechanics: Fundamentals and Applications, Third Edition.” CRC Press, 2005.

[46] Talari, M. K., Babu, K.N., Kallip, K., Leparoux, M., Koller, R. E., AlOgab, K. A. and Maeder, X. “Microstructure, Mechanical, and Impression Creep Properties of AlMg5–0.5 vol% Al2O3 Nanocomposites”, Adv. Eng. Mater., 2016, 18: 1958–1966.

[47] Poirier, D., Drew, R. A. L., Trudeau, M. L., Gauvin, R., “Fabrication and properties of mechanically milled alumina/aluminum nanocomposites,” Mater. Sci. Eng. A, 2010, vol. 527, no. 29–30, pp. 7605–7614.

[48] Tavoosi, M., Karimzadeh, F., Enayati, M. H., Heidarpour, A., “Bulk Al–Zn/Al2O3 nanocomposite prepared by reactive milling and hot pressing methods,” J. Alloys Compd., 2009, vol. 475, no. 1–2, pp. 198–201.

[49] Lee, Z., Witkin, D. B., Radmilovic, V., Lavernia, E. J., Nutt, S. R., “Bimodal microstructure and deformation of cryomilled bulk nanocrystalline Al–7.5Mg alloy,” Mater. Sci. Eng. A, 2005, vol. 410–411, pp. 462–467.

[50] Mittemeijer, E. J., “Fundamentals of Materials Science.” Berlin, Heidelberg: Springer Berlin Heidelberg, 2011.

[51] Wagih, A., “Mechanical properties of Al–Mg/Al2O3 nanocomposite powder produced by mechanical alloying,” Adv. Powder Technol., 2015, vol. 26, no. 1, pp. 253–258.

[52] Serdechnova, M., Kallip, S., Ferreira, M. G. S., Zheludkevich, M. L., “Active self-healing coating for galvanically coupled multi-material assemblies,” Electrochem. Commun., 2014, vol. 41, pp. 51–54.

[53] Balog, M., Hu, T., Krizik, P., Riglos, M.V.C., Saller, B.D., Yang, H., Schoenung, J.M., Lavernia, E.J., “On the thermal stability of ultrafine-grained Al stabilized by in-situ amorphous Al2O3 network,” Mater. Sci. Eng. A, 2015, vol. 648, pp. 61–71.

[54] ASM Specialty Handbook: Aluminum and Aluminum Alloys - ASM International. 1993.

[55] Ma, K., Wen, H., Hu, T., Topping, T.D., Isheim, D., Seidman, D.N., Lavernia, E.J., Schoenung, J.M., “Mechanical behavior and strengthening mechanisms in ultrafine grain precipitation-strengthened aluminum alloy,” Acta Mater., 2014, vol. 62, pp. 141–155.

[56] Babu, N. K., Kallip, K., Leparoux, M., AlOgab, K. A., Reddy, G. M., Talari, M. K., “Characterization of microstructure and mechanical properties of friction stir welded AlMg5- Al2O3 nanocomposites,” Mater. Sci. Eng. A, 2016, vol. 658, pp. 109–122.

LIST OF MAIN PUBLICATIONS

- Kallip, K., Kollo, L., Leparoux, M., & Bradbury, C., “Nanoparticulate Reinforced Aluminum Alloy Composites Produced by Powder Metallurgy Route.” In *Advanced Composites for Aerospace, Marine, and Land Applications II,* 2015, 165-174. Springer International Publishing.

- Kallip, K., Leparoux, M., AlOgab, K. A., Clerc, S., Deguilhem, G., Arroyo, Y., & Kwon, H., “Investigation of different carbon nanotube reinforcements for fabricating bulk AlMg5 matrix nanocomposites.” *Journal of Alloys and Compounds*, 2015, *646*, 710-718.

- Kallip, K., Babu, N. K., AlOgab, K. A., Kollo, L., Maeder, X., Arroyo, Y., & Leparoux, M., “Microstructure and mechanical properties of near net shaped aluminium/alumina nanocomposites fabricated by powder metallurgy.” *Journal of Alloys and Compounds*, 2017, *714*, 133-143.

- Babu, N. K., Kallip, K., Leparoux, M., AlOgab, K. A., Maeder, X., & Dasilva, Y. A. R., “Influence of microstructure and strengthening mechanism of AlMg5–Al 2 O 3 nanocomposites prepared via spark plasma sintering.” *Materials & Design*, 2016, *95*, 534-544.

ACKNOWLEDGEMENTS

This work is based on the experimental work carried out in the labs of EMPA and Tallinn University of Technology.

Above all, I would like to express my special thanks to my supervisors Dr. Lauri Kollo and Dr. Marc Leparoux for their support, guidance and encouragement which made this work possible.

I am deeply grateful to all of my colleagues at EMPA for their endless support and scientific discussions. The opportunity to be a part of this wonderful team was a truly unique and valuable experience. My deepest gratitude's are going to Prof. Patrik Hoffmann and Dr. Johann Michler, the heads of the laboratories in EMPA Thun for inviting me to their labs and mentoring and advising me with fruitful scientific discussions.

It is impossible for me to overestimate the contribution of every single person in abt. 204 and abt. 206 in EMPA and my colleagues at Tallinn University of Technology. I want to thank every one of you for helping me at experimental procedures, theoretical work and scientific discussions or just having good time after work.

I would also like to thank Bernhard von Gunten, Anton Böll, Peter Ramseier and Hans Vallner for all the help during sample preparation, fabrication and testing. I would like to thank Gerhard Bürki, Dr. Yadira Arroyo, Dr. Xavier Maeder, Dr. Aidan Taylor, Dr James Best, Dr Fatemeh Saeidi, Dr. Sriharitha Rowthu and Marie Le Dantec for introducing me to the different interesting characterization methods.

I would also like to thank Dr. Khaled Al.Ogab and KACST for their invaluable scientific and financial support.

This work was funded by King Abdulaziz City for Science and Technology (KACST). This work was also funded by Institutional Research Funding project IUT19-29, targeted funding project SF0140062s08 and Estonian Science Foundation Research Grant project ETF8472. This work has also been partially supported by ASTRA "TUT Institutional Development Program for 2016-2022" Graduate School of Functional Materials and Technologies (2014-2020.4.01.16-0032)

Finally, I would like to thank my family and friends for their continuous support, patience, understanding and encouragement at different stages of the present work.

ABSTRACT

High strength ductile aluminium matrix composite.

The need for stronger and lighter materials have increased over time and therefore this topic is under interest of many researchers now more than ever before. The limitations of metal alloying to provide required strength and stiffness to engineering material have led to research and usage of composite materials. Metal matrix composites have found their place in industry as high-tech engineering materials even though a lot of developments are still to be performed to improve the material.

The chosen matrix, type and size of reinforcement, the method of reinforcement distribution and different post processing methods are only few possibilities to tailor the material with desired engineering properties for application. With reduction of the reinforcement size down to nanometre scale number of properties are expansively enhanced.

Current research is concentrated on the development of novel aluminium based metal matrix nanocomposite with simultaneous high strength and ductility. Additionally the aim is to achieve the desired performance of material with minimal processing steps to simplify the fabrication.

The thesis consists of three main studies including improvement of hardness and strength of MMC, obtaining simultaneous strength and ductility and the investigation to find the optimum compaction method for acquired powder metallurgical MMC. As a result of these studies high ultimate tensile strength of 720 MPa was achieved for 0.5 vol% MWCNT reinforced AlMg5 alloy, but the material presented modest ductility of about 1%. Optimizing of the milling process and the type of reinforcement allowed to create the material with compromised parameters. The tensile strength of 470 MPa with simultaneous elongation exceeding 11% is certainly by far outperforming the strength properties of non-heat treated aluminium alloys, which is achieved through hot pressing aluminium based-MMC and which can be produced with simple one step processing directly into near net shaped objects.

KOKKUVÕTE

Kõrgtugev ja plastne alumiinium komposiitmaterjal.

Läbi aegade on olnud kõrge vajadus kergemate ja tugevamate materjalide järgi, mis on inspireerinud rohkelt teadusuuringuid. Ajalooliselt on metallsete materjalide parendamine käinud legeerimise teel sulamite valmistamisena. Kuna aga sulamite legeerimisel on teatavad piirangud, mis takistavad saavutamast parimaid tugevuse ja sitkuse kombineeringuid, on viimasel ajal peamised uuringud suundunud komposiitmaterjalide arendamisele. Metallmaatriks komposiitmaterjalid on leidnud oma koha tööstuses kui kõrgtehnoloogilised materjalid, aga sellegipoolest on veel palju mida nende materjalide juures parendada annab.

Käesolev uurimustöö on fokuseeritud uudse alumiiniumi baasil nanokomposiitmaterjali arendamisele. Töö eesmärgiks on seatud, et arendatav komposiitmaterjal oleks üheaegselt nii kõrgtugev kui ka plastne. Piisavalt plastne, et materjal oleks kasutatav tööstusmaterjalina. See tähendab tööstuses üldlevinud arusaamade kohaselt katkevenivust üle 4%. Lisaks peavad materjali tugevusomadused olema saavutatud minimaalsete protsessi sammudega lihtsustamaks materjali valmistamist.

Valitud maatriksi ja armeeringu tüüp ning suurus, aremeeringu ühtlase maatriksisse jaotamise meetod ja erinevad järeltöötlusprotsessid on ainult mõned võimalikest moodustest loomaks sobivate omadustega komposiitmaterjal. Lisaks on armeeringu suuruse vähendamisega nanosuurustesse võimalik erinevaid materjali omadusi eksponentsiaalselt parendada.

Antud uurimustöö käsitleb kolme peateemat milleks on materjali kõvaduse ja tugevuse tõstmine, materjali kõrgtugevuse ja plastsuse üheaegne saavutamine ning optimaalse tihendamismeetodi leidmine pulbermetallurgilisele komposiidile. Töös saavutati 720 MPa maksimaalset tõmbetugevust 0.5 mahu% süsinik nanotrudega armeeritud AlMg5 sulamil põhineva komposiidi puhul. Saavutatud tugevuse juures jäi aga katkevenivus umbes 1 % juurde. Optimeerides jahvatusprotsessi ja armeeringmaterjali tüüpi saavutati materjal mis omas üheaegselt 470 MPa tõmbetugevust ja 11 % katkevenivust. Saavutatud omadused ületavad kindlalt kuumpressitud külmtöödeldavate alumiiniumsulamite tugevusomadused. Valmistatud materjali omadused teeb märkimisväärseks, et need on saavutatud üheastmelise kuumpressimisega otse lõppkujuga detailideks ilma vajaduseta järeltöötlusprotsessideks.

CURRICULUM VITAE

1. Personal data

Name and surname	Kaspar Kallip
Date and place of birth	July 14, 1986, Rakvere, Estonia
Nationality	Estonian
E-mail address	kaspar.kallip@gmail.com

2. Education

Educational institution (name during graduation)	Graduation	Education (degree)
Tallinn University of Technology	2012	Master of Science
Tallinn University of Technology	2010	Bachelor of Science
Rakvere Reaalgpmnaasium	2005	Secondary education

3. Language skills (basic, good, fluent)

Language	Skill
Estonian	Fluent
English	Fluent
Russian	Basic
German	Basic

4. Additional training

Training period	Additional training facility
2010–2011	EMPA Masters study training
2013–2015	EMPA PhD student training

5. Professional employment

Period	Employer	Position
2011– *to date*	Tallinn University of Technology	Early stage researcher

6. Research activities and supervised theses

Projects	IUT19-29 "Multi-scale structured ceramic-based composites for extreme applications (1.01.2014−31.12.2019)", Jakob Kübarsepp, Tallinn University of Technology , Faculty of Mechanical Engineering, Tallinn University of Technology , School of Engineering, Department of Mechanical and Industrial Engineering
	AR12131 "Permanent magnets for sustainable energy application (MagMat). (17.03.2012−30.06.2015)", Renno Veinthal, Tallinn University of Technology , Tallinn University of Technology , Faculty of Mechanical Engineering, Department of Materials Engineering , Tallinn University of Technology , Faculty of Power Engineering, Department of Electrical Engineering.
	SF0140062s08 "Design and technology of multiphase tribomaterials (1.01.2008−31.12.2013)", Jakob Kübarsepp, Tallinn University of Technology , Faculty of Mechanical Engineering.
	ETF8472 "Metal Matrix Nanocomposites - reinforcement with nanoparticles of different processing history (1.01.2010−31.12.2012)", Lauri Kollo, Tallinn University of Technology , Faculty of Mechanical Engineering.
Patents	Method and device for manufacturing sintered material products; Owner: Tallinn University of Technology; Authors: Lauri Kollo, Kaspar Kallip, Zorjana Mural, Hans Vallner, Renno Veinthal, Märt Kolnes, Marek Tarraste, Marek Jõeleht; Priority number: P201500021; Priority date: May 13, 2015
Supervised theses	Master thesis „ Additive manufacturing of aluminium alloys and composites “ Raido Pajussaar

ELULOOKIRJELDUS

1. Isikuandmed

Ees- ja perekonnanimi	Kaspar Kallip
Sünniaeg ja -koht	14 juuli 1986, Rakvere, Eesti
Kodakondsus	Eesti
E-posti aadress	kaspar.kallip@gmail.com

2. Hariduskäik

Õppeasutus (nimetus lõpetamise ajal)	Lõpetamise aasta	Haridus (eriala/kraad)
Tallinna Tehnikaülikool	2012	Tehnikateaduse magister
Tallinna Tehnikaülikool	2010	Tehnikateaduse bakalaureus
Rakvere Reaalgümnaasium	2005	Keskharidus

3. Keelteoskus (alg-, kesk- või kõrgtase)

Keel	Tase
Eesti	Kõrgtase (emakeel)
Inglise	Kõrgtase
Vene	Kesktase
Saksa	Algtase

4. Täiendusõpe

Õppimise aeg	Täiendusõppe korraldaja nimetus
2010–2011	EMPA Praktikant
2013–2015	EMPA Doktorant

5. Teenistuskäik

Töötamise aeg	Tööandja nimetus	Ametikoht
2011– *praeguseni*	Tallinna Tehnikaülikool	Nooremteadur

6. Teadustegevus ja juhendatud lõputööd

Projektid	IUT19-29 " Mitmeastmeliselt struktureeritud keraamika-baasil komposiitmaterjalid kasutamiseks ekstreemtingimustes (1.01.2014−31.12.2019)", Jakob Kübarsepp, Tallinna Tehnikaülikool, Mehaanikateaduskond, Tallinna Tehnikaülikool, Inseneriteaduskond, Mehaanika ja tööstustehnika instituut . AR12131 " Püsimagnetid jätkusuutliku energeetika rakendustes (MagMat).“ (17.03.2012−30.06.2015)", Renno Veinthal, Tallinna Tehnikaülikool, Tallinna Tehnikaülikool, Mehaanikateaduskond, Materjalitehnika instituut, Tallinna Tehnikaülikool, Energeetikateaduskond, Elektrotehnika instituut SF0140062s08 "Mitmefaasiliste tribomaterjalide arendamine ja tehnoloogia (1.01.2008−31.12.2013)", Jakob Kübarsepp, Tallinna Tehnikaülikool, Mehaanikateaduskond. ETF8472 "Nanoosakeste valmistustehnoloogia mõju metallmaatriks nanokomposiitide omadustele (1.01.2010−31.12.2012)", Lauri Kollo, Tallinna Tehnikaülikool, Mehaanikateaduskond.
Patendid	Meetod ja seade pulbermaterjalist toodete valmistamiseks; Omanik: Tallinna Tehnikaülikool; Autorid: Lauri Kollo, Kaspar Kallip, Zorjana Mural, Hans Vallner, Renno Veinthal, Märt Kolnes, Marek Tarraste, Marek Jõeleht; Prioriteedi number: P201500021; Prioriteedi kuupäev: 13.05.2015
Juhendatud lõputööd	Magistritöö „Alumiiniumsulamite ja komposiitide kihtlisandustehnoloogiline valmistamine“ Raido Pajussaar

DISSERTATIONS DEFENDED AT TALLINN UNIVERSITY OF TECHNOLOGY ON *MECHANICAL ENGINEERING*

1. **Jakob Kübarsepp**. Steel-Bonded Hardmetals. 1992.

2. **Jakub Kõo**. Determination of Residual Stresses in Coatings &Coated Parts. 1994.

3. **Mart Tamre**. Tribocharacteristics of Journal Bearings Unlocated Axis. 1995.

4. **Paul Kallas**. Abrasive Erosion of Powder Materials. 1996.

5. **Jüri Pirso**. Titanium and Chromium Carbide Based Cermets. 1996.

6. **Heinrich Reshetnyak**. Hard Metals Serviceability in Sheet Metal Forming Operations. 1996.

7. **Arvi Kruusing**. Magnetic Microdevices and Their Fabrication methods. 1997.

8. **Roberto Carmona Davila**. Some Contributions to the Quality Control in Motor Car Industry. 1999.

9. **Harri Annuka**. Characterization and Application of TiC-Based Iron Alloys Bonded Cermets. 1999.

10. **Irina Hussainova**. Investigation of Particle-Wall Collision and Erosion Prediction. 1999.

11. **Edi Kulderknup**. Reliability and Uncertainty of Quality Measurement. 2000.

12. **Vitali Podgurski**. Laser Ablation and Thermal Evaporation of Thin Films and Structures. 2001.

13. **Igor Penkov**. Strength Investigation of Threaded Joints Under Static and Dynamic Loading. 2001.

14. **Martin Eerme**. Structural Modelling of Engineering Products and Realisation of Computer-Based Environment for Product Development. 2001.

15. **Toivo Tähemaa**. Assurance of Synergy and Competitive Dependability at Non-Safety-Critical Mechatronics Systems design. 2002.

16. **Jüri Resev**. Virtual Differential as Torque Distribution Control Unit in Automotive Propulsion Systems. 2002.

17. **Toomas Pihl**. Powder Coatings for Abrasive Wear. 2002.

18. **Sergei Letunovitš**. Tribology of Fine-Grained Cermets. 2003.

19. **Tatyana Karaulova**. Development of the Modelling Tool for the Analysis of the Production Process and its Entities for the SME. 2004.

20. **Grigori Nekrassov**. Development of an Intelligent Integrated Environment for Computer. 2004.

21. **Sergei Zimakov**. Novel Wear Resistant WC-Based Thermal Sprayed Coatings. 2004.

22. **Irina Preis**. Fatigue Performance and Mechanical Reliability of Cemented Carbides. 2004.

23. **Medhat Hussainov**. Effect of Solid Particles on Turbulence of Gas in Two-Phase Flows. 2005.

24. **Frid Kaljas**. Synergy-Based Approach to Design of the Interdisciplinary Systems. 2005.

25. **Dmitri Neshumayev**. Experimental and Numerical Investigation of Combined Heat Transfer Enhancement Technique in Gas-Heated Channels. 2005.

26. **Renno Veinthal**. Characterization and Modelling of Erosion Wear of Powder Composite Materials and Coatings. 2005.

27. **Sergei Tisler**. Deposition of Solid Particles from Aerosol Flow in Laminar Flat-Plate Boundary Layer. 2006.

28. **Tauno Otto**. Models for Monitoring of Technological Processes and Production Systems. 2006.

29. **Maksim Antonov**. Assessment of Cermets Performance in Aggressive Media. 2006.

30. **Tatjana Barashkova**. Research of the Effect of Correlation at the Measurement of Alternating Voltage. 2006.

31. **Jaan Kers**. Recycling of Composite Plastics. 2006.

32. **Raivo Sell**. Model Based Mechatronic Systems Modeling Methodology in Conceptual Design Stage. 2007.

33. **Hans Rämmal**. Experimental Methods for Sound Propagation Studies in Automotive Duct Systems. 2007.

34. **Meelis Pohlak**. Rapid Prototyping of Sheet Metal Components with Incremental Sheet Forming Technology. 2007.

35. **Priidu Peetsalu**. Microstructural Aspects of Thermal Sprayed WC-Co Coatings and Ni-Cr Coated Steels. 2007.

36. **Lauri Kollo**. Sinter/HIP Technology of TiC-Based Cermets. 2007.

37. **Andrei Dedov**. Assessment of Metal Condition and Remaining Life of In-service Power Plant Components Operating at High Temperature. 2007.

38. **Fjodor Sergejev**. Investigation of the Fatigue Mechanics Aspects of PM Hardmetals and Cermets. 2007.

39. **Eduard Ševtšenko**. Intelligent Decision Support System for the Network of Collaborative SME-s. 2007.

40. **Rünno Lumiste**. Networks and Innovation in Machinery and Electronics Industry and Enterprises (Estonian Case Studies). 2008.

41. **Kristo Karjust**. Integrated Product Development and Production Technology of Large Composite Plastic Products. 2008.

42. **Mart Saarna**. Fatigue Characteristics of PM Steels. 2008.

43. **Eduard Kimmari**. Exothermically Synthesized B_4C-Al Composites for Dry Sliding. 2008.

44. **Indrek Abiline**. Calibration Methods of Coating Thickness Gauges. 2008.

45. **Tiit Hindreus**. Synergy-Based Approach to Quality Assurance. 2009.

46. **Karl Raba**. Uncertainty Focused Product Improvement Models. 2009.

47. **Riho Tarbe**. Abrasive Impact Wear: Tester, Wear and Grindability Studies. 2009.

48. **Kristjan Juhani**. Reactive Sintered Chromium and Titanium Carbide-Based Cermets. 2009.

49. **Nadežda Dementjeva**. Energy Planning Model Analysis and Their Adaptability for Estonian Energy Sector. 2009.

50. **Igor Krupenski**. Numerical Simulation of Two-Phase Turbulent Flows in Ash Circulating Fluidized Bed. 2010.

51. **Aleksandr Hlebnikov**. The Analysis of Efficiency and Optimization of District Heating Networks in Estonia. 2010.

52. **Andres Petritšenko**. Vibration of Ladder Frames. 2010.

53. **Renee Joost**. Novel Methods for Hardmetal Production and Recycling. 2010.

54. **Andre Gregor**. Hard PVD Coatings for Tooling. 2010.

55. **Tõnu Roosaar**. Wear Performance of WC- and TiC-Based Ceramic-Metallic Composites. 2010.

56. **Alina Sivitski**. Sliding Wear of PVD Hard Coatings: Fatigue and Measurement Aspects. 2010.

57. **Sergei Kramanenko**. Fractal Approach for Multiple Project Management in Manufacturing Enterprises. 2010.

58. **Eduard Latõsov**. Model for the Analysis of Combined Heat and Power Production. 2011.

59. **Jürgen Riim**. Calibration Methods of Coating Thickness Standards. 2011.

60. **Andrei Surzhenkov**. Duplex Treatment of Steel Surface. 2011.

61. **Steffen Dahms**. Diffusion Welding of Different Materials. 2011.

62. **Birthe Matsi**. Research of Innovation Capasity Monitoring Methodology for Engineering Industry. 2011.

63. **Peeter Ross**. Data Sharing and Shared Workflow in Medical Imaging. 2011.

64. **Siim Link**. Reactivity of Woody and Herbaceous Biomass Chars. 2011.

65. **Kristjan Plamus**. The Impact of Oil Shale Calorific Value on CFB Boiler Thermal Efficiency and Environment. 2012.

66. **Aleksei Tšinjan**. Performance of Tool Materials in Blanking. 2012.

67. **Martinš Sarkans**. Synergy Deployment at Early Evaluation of Modularity of the Multi-Agent Production Systems. 2012.

68. **Sven Seiler**. Laboratory as a Service – A Holistic Framework for Remote and Virtual Labs. 2012.

69. **Tarmo Velsker**. Design Optimization of Steel and Glass Structures. 2012.

70. **Madis Tiik**. Access Rights and Organizational Management in Implementation of Estonian Electronic Health Record System. 2012.

71. **Marina Kostina**. Reliability Management of Manufacturing Processes in Machinery Enterprises. 2012.

72. **Robert Hudjakov**. Long-Range Navigation for Unmanned Off-Road Ground Vehicle. 2012.

73. **Arkadi Zikin**. Advanced Multiphase Tribo-Functional PTA Hardfacings. 2013.

74. **Alar Konist**. Environmental Aspects of Oil Shale Power Production. 2013.

75. **Inge Roos**. Methodology for Calculating CO_2 Emissions from Estonian Shale Oil Industry. 2013.

76. **Dmitri Shvarts**. Global 3D Map Merging Methods for Robot Navigation. 2013.

77. **Kaia Lõun**. Company's Strategy Based Formation of e-Workplace Performance in the Engineering Industry. 2013.

78. **Maido Hiiemaa**. Motion Planner for Skid-Steer Unmanned Ground Vehicle. 2013.

79. **Dmitri Goljandin**. Disintegrator Milling System Development and Milling Technologies of Different Materials. 2013.

80. **Dmitri Aleksandrov**. Light-Weight Multicopter Structural Design for Energy Saving. 2013.

81. **Henrik Herranen**. Design Optimization of Smart Composite Structures with Embedded Devices. 2014.

82. **Heiki Tiikoja**. Experimental Acoustic Characterization of Automotive Inlet and Exhaust System. 2014.

83. **Jelena Priss**. High Temperature Corrosion and Abrasive Wear of Boiler Steels. 2014.

84. **Aare Aruniit**. Thermoreactive Polymer Composite with High Particulate Filler Content. 2014.

85. **Dmitri Gornostajev**. Development of the Calculation Method for Barge Hull. 2014.

86. **Liina Lind**. Wear of PVD Coatings on Fineblanking Punches. 2014.

87. **Nikolai Voltšihhin**. Design and Technology of Oxides-Containing Ceramic-Based Composites. 2014.

88. **Aleksander Šablinski**. RANS Numerical Modelling of Turbulent Polydispersed Flows in CFB Freeboard. 2015.

89. **Tanel Aruväli**. Wireless Real-time Monitoring of Machining Processes. 2015.

90. **Andrei Bogatov**. Morphological Changes on Diamond and DLC Films During Sliding Wear. 2015.

91. **Raimo Kabral**. Aero-Acoustic Studies and Innovative Noise Control with Application to Modern Automotive Gas Exchange System. 2015.

92. **Jevgeni Sahno**. Dynamic Management Framework for Continuous Improvement of Production Processes. 2015.

93. **Ott Pabut**. Optimal Design of Slotless Permanent Magnet Generators. 2015.

94. **Merili Kukuškin**. Value Centric Business Development for Estonian Manufacturing Small and Medium Sized Enterprises. 2015.

95. **Kaimo Sonk**. Development of Additive Manufacturing Based on Functional Requirements. 2015.

96. **Marina Aghayan**. Functionalization of Alumina Nanofibers with Metal Oxides. 2016.

97. **Marek Jõeleht**. Titanium Carbide Cermet as Ballistic Protection Material. 2016.

98. **Heikki Sarjas**. Novel Synthesized and Milled Carbide-based Composite Powders for HVOF Spray. 2016.

99. **Klodian Dhoska**. Measurement Methods with 3D Coordinate Measuring Machine and Improved Characterization Setup for Detector Performance. 2016.

100. **Aleksei Snatkin**. Development and Optimisation of Production Monitoring System. 2016.

101. **Igor Poljantšikov**. Partners Selection Tool for Virtual Enterprise in SMEs Network. 2016.

102. **Sergei Žigailov**. Experimental and Analytical Modelling of Pelvic Motion. 2016.

103. **Rommi Källo**. Synergy-Based Chaos Control in the Multi-Agent Hierarchical Systems. 2016.

104. **Der-Liang Yung**. ZrC-based and ZrC-doped Composites for High-Temperature and Wear Applications. 2016.

105. **Viive Pille**. Development of a Model for the Prevention of Work-Related Musculoskeletal Disorders in the Upper Extremities. 2016.

106. **Agus Pramono**. Investigation of Severe Plastic Deformation Processes for Aluminum Based Composites. 2016.

107. **Zorjana Mural**. Technology and Properties of Fine-grained Nd-Fe-B Magnets. 2017.

108. **Eero Väljaots**. Energy Efficiency Evaluation Method for Mobile Robot Platform Design. 2017.

109. **Viktoria Baškite**. Decision-Making Tool Development for Used Industrial Equipment Life Cycle Evaluation and Improvement. 2017.